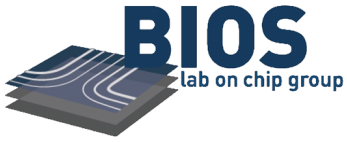

UNIVERSITY OF TWENTE.

Parallel sampling from individual cells on a microchip:

towards a parallel single cell analysis platform

MASTER THESIS
ELECTRICAL ENGINEERING

F.T.G. van den Brink
0072885

REPORT NUMBER: 2011-2 BIOS

ENSCHEDE, FEBRUARY 3, 2011

BIOS/Lab on a chip group
Faculty of Electrical Engineering, Mathematics and Computer Science
University of Twente, The Netherlands

Graduation committee:

Prof. dr. ir. A. van den Berg
dr. ir. Séverine Le Gac
dr. E.T. Carlen
Prof. dr. L.W.M.M. Terstappen

Abstract

Cell populations are heterogeneous: processes are not synchronized in a cell population and individual cells are at different stages of the cell cycle, for instance. Consequently, conventional analysis methods provide averaged information about the cell population as an ensemble and this does not give useful information about the state of individual cells. A single cell analysis approach looks more attractive in that respect; however, the analysis of a single cell in a population appears to be a biased approach as one cannot extrapolate this information to the state of the population. Therefore, a more relevant approach consists of analyzing cells of a population in an individual manner, so as to collect information not only at the single cell level but also at the population level. This approach reveals the population heterogeneity, which is thought to be indicative of disease development.

In this work, a microfluidic platform is described for this purpose. This microchip is intended as a first prototype to enable proof-of-principle experiments towards actual parallel single cell analysis. The whole analysis process consists of four steps. First, individual living cells are trapped individually in a controlled and reproducible way. Second, the plasma membrane is permeabilized, either transiently or irreversibly. Third, the cell content of individual cells is extracted in a controlled way and fourth, the analysis is performed on the extracted biomolecules.

A PDMS microsystem is developed to perform the first three steps of the analysis protocol. The microsystem contains an array of 16 trapping structures for the immobilization of 16 individual cells in parallel by accurate application of a negative pressure across these structures. A single cell trapping efficiency of > 90% is demonstrated with the aforementioned protocol and optimal dimensions of the trapping structures. Trapping is fast, controllable, reproducible, efficient and scalable. Cells are permeabilized through their exposure to a plug of chemicals, such as digitonin (3.5 min incubation) for reversible permeabilization or lithium dodecylsulphate (LiDS) for irreversible lysis (10-20 s exposure). Cell permeabilization is monitored via the release of calcein out of the cells and the entry of PI, two membrane-impermeable dyes. Interestingly, the way the cell is trapped has a high impact on this permeabilization step, while the cell trapping mode cannot be controlled. Alternatively, cell lysis is demonstrated using an electric field; there, the cell trapping mode has no detectable influence on the permeabilization process. Finally, an electroosmotic flow (EOF) is established in the individual side channels located behind the trapped cells for extraction of the cell content in there. This last step is illustrated with the controlled extraction of calcein out of the cells, for both reversible and irreversible chemical permeabilization.

Contents

Acknowledgements

Here I would like to thank all the people who have contributed to this project.

Prof. Albert van den Berg, as the head of the BIOS Lab-on-a-Chip group, made it possible for me to do this assignment within BIOS. Thank you for giving me the chance to work here.

Séverine Le Gac, my supervisor, has supported me a lot during this project. We had many interesting meetings in which you had a lot of helpful ideas and insights. Also, you have helped me improving my writing and presentation skills significantly. Thank you, it has been a year in which I have gained a lot of new scientific knowledge and experience.

Edwin Carlen and Prof. Leon Terstappen, thank you for participating in my graduation committee. I appreciate you have time to take part in my master thesis work.

Eddy de Weerd has introduced me to the fabrication of PDMS chips. Thank you for that, and for having time to answer many other questions.

The technicians within BIOS have provided very essential support during this project. Paul ter Braake, head of the Cell Lab, has introduced me to this lab and he supported me with the cell culturing. Johan Bomer has fabricated the molds in the cleanroom, which are used for the production of the PDMS chips. Hans de Boer has engineered a customized microscope stage for my experimental setup. Henk van Wolferen and Jan van Nieuwkasteele have introduced me to the microscope and supported me with this during the project. All of you: thanks a lot for the assistance and contributions.

Verena Stimberg, thank you for explaining me how to analyze my data with ImageJ. It would be difficult to draw hard conclusions from the fluorescence images if I cannot quantify something in there.

Anja Stefanovic has introduced me in the very beginning to my measurement setup. Thank you for getting me started there.

Thanks to all the BIOS group members, for the good discussions and nice atmosphere. You are fantastic colleagues to work with.

1 Introduction

1.1 Cell analysis

Cells are the basic units of life and they have the ability to replicate themselves. The cell's functioning is determined by biomolecules, which are the nucleic acids, proteins, polysaccharides and lipids. Every cell contains the full genome of the organism it belongs to. This genome contains the hereditary information that is needed for its replication and differentiation. The information is encoded in DNA, which consists of nucleic acids. Proteins are the products of gene expression and they are produced in two steps. First, the DNA is transcribed into mRNA, which is another nucleic acid. Second, the mRNA is translated into the protein. The proteins serve functions in various cellular processes, such as cell communication and the transcription and translation activities. Polysaccharides are involved in the cellular metabolism, providing the cell with energy. Finally, lipids are the main building blocks of membranes. Both the cell information and activity are compartmentalized in organelles. For example, the genome is stored in the nucleus and the cell's energy production is carried out in mitochondria.

The molecular biology as we know it nowadays started in the 60's. Within this field, cell analysis is carried out on the level of populations and tissues. The standard approach for population analysis since that time is flow cytometry. Cell analysis along this strategy brings statistical data, which is relevant at the level of the cell population. However, the information obtained with an analysis is also averaged on the whole population.

In the 90's, microfluidic tools became available for single cell analysis (SCA) with structrures developed for the isolation and manipulation of individual cells. With this technology, analysis of single cell behaviour is possible on the cell's phenotype or the amount of different types of biomolecules. However, this information is biased since the behaviour of an isolated single cell cannot be extrapolated to the population it belongs to. Cell populations are heterogenous, due to stochastic fluctuations of the molecular processes that are involved in the cell's functioning (biological noise), such as the RNA transcription from DNA, the protein translation from RNA and the degradation of biomolecules [1].

These two cell analysis strategies, at the population and the single cell level, are complementary and both provide useful information. Single cell behaviour from a representative sample of the population is needed and for this, cell analysis has to be carried out with a large number of isolated single cells in parallel. This approach combines the benefits of both the population studies and the single cell analysis, while leaving out their disadvantages. Using a large number of cells reduces the biological noise, thereby increasing the quality of the data analysis at the single cell level. With this approach, information can also be retreived about the heterogeneity of cell populations, providing new research opportunities. The microfluidic technology has been evolving rapidly since its introduction in the 1990's and this can be applied for the realization of a parallel SCA platform. Table 1 summarizes the advantages and disadvantages of the three aforementioned cell analysis approaches.

Table 1: Comparison of the cell analysis approaches on their advantages and disadvantages with respect to the information obtained about cell behaviour.

Analysis approach	Advantages	Disadvantages
Population analysis	Statistical information	Avarage over population
Single cell analysis	Single cell behaviour	Biased information
Parallel single cell analysis	Statistical data + single cell behaviour	-

Parallel SCA can be used for many diagnostic applications [2]. In stem cell research for example, cells can be analyzed to obtain information about signaling pathways for self renewal and differentiation. Especially the field of systems biology, that aims at characterizing all of the components in cellular systems will benefit from parallel SCA developments. With the emergence of analysis techniques that address single cells in a population, the heterogeneity of the

population provides new information instead of noise and through a better understanding of this phenomenon, ultimately this knowledge of cellular processes can be applied for the development of methods that minimize this heterogeneity in engineered biological systems [3].

When microfluidics is used for realizing a parallel SCA system, new research opportunities are provided and this will become even more interesting if minimally invasive handling and analysis procedures are developed. For example, the study of cellular reactions to gene transfection in the form of protein expression at the single cell level requires a transfection step that keeps the cell alive because it has to process the injected compounds. Other possible research topics of this type are cell signaling and cell metabolism studies. For these dedicated applications, the environment in which the cell is processed has a great influence on the experimental success and therefore it is important to choose the right experimental platform.

1.2 Microfluidics for biological systems

The field of microfluidics aims at developing systems that can manipulate fluid in the low microliter range in channels with dimensions of tens to hundreds of micrometers [4]. This technology offers many useful capabilities for analysis purposes. The small dimensions of the structures that are used to handle liquids have the advantage of a very low consumption of chemicals compared to traditional analysis systems, which also results in lower amounts of waste. Furthermore, these dimensions allow a fast analysis due to the short diffusion distances. Also, the high surface-to-volume ratio leads to the development of laminar flows, allowing accurate manipulation of analytes in space and time. These advantages contributed to the development of microfluidic platforms for biological and chemical analysis under the name of of lab-on-a-chip (LOC) technology.

The LOC systems are produced on chips with mm^2 to cm^2 dimensions, which is interesting for applications in portable devices that are used for point-of-care, in situ, or environmental analysis. These chips can be fabricated from materials that allow large scale production (glass, silicon or most polymers), which leads to low fabrication costs and therefore the devices themselves can be used as disposables, avoiding the need for system regeneration. The fabrication processes originate in the microelectronics industry and they involve high precision technologies. Therefore, the materials and processes are available to fabricate the microfluidic systems with highly uniform characteristics, which is a basic condition for reproducible analysis.

Analysis systems on chip are amenable to a high degree of integration by performing multiple operations in series or in parallel. Vertical integration provides shorter analysis times and better analysis reproducibility, because no intermediate sample handling is required between the integrated analysis steps. This also reduces the risk of sample contamination and sample loss, and the analysis conditions in the system can be controlled precisely for every operation. Horizontal integration increases the output of the system by using parallelization of operations. Ultimately, automation of the analysis is possible and beneficial if a high degree of both types of integration are achieved.

A system that is to be used for parallel SCA can only be realized successfully using LOC technology. A typical mammalian cell has a diameter of 10-20 μm and a volume in the picoliter range. The size of the structures in microfluidic devices are similar to the size of the cells that have to be analyzed, which is favourable for cell handling and single cell isolation [5]. Also, both the benefits of horizontal and vertical integration can be exploited. The first to scale up, providing oportunities for the analysis of a large number of cells in parallel and the second to integrate multiple functionalities in the platform for additional tasks, such as sensing of biomolecules.

Working with cells, having micrometer dimensions and picoliter volumes, imposes certain requirements on the platform that performs the analysis. The cells have to be immobilized at a certain position and the species of interest need to be extracted and transported for analysis. This requires control of the conditions in the microenvironment of the cell and the ability to direct the cells and the analytes to a well-defined location. Furthermore, the extracted analytes will come with a very low amount, typically 1-100 copies/cell for nucleic acids and proteins. Therefore, it is

important to minimize the dilution of the sample and to employ a highly sensitive detection system with single molecule capability, which is also a current key research topic in LOC technology.

1.3 Parallel single cell analysis on a microfluidic chip

A LOC system for parallel SCA has to fulfill the following tasks:

1. Immobilizing a large number of individual cells in parallel.
2. Providing access to the intracellular environment.
3. Transporting cellular compounds to an analysis site.
4. Analysis of the extracted sample.

These steps will be further explained in this chapter and illustrated with examples found in the literature.

1.3.1 Cell trapping

The first step that has to be completed by the parallel SCA system is the immobilization of individual cells in parallel at well-defined locations. Traditionally, this is accomplished by localized surface modification or with chemical immobilization in a perfused system, but these methods are not optimal for applications in which the cells have to survive. New developments have resulted in a variety of LOC platforms with trapping functionality for the control of cells on a chip [6]. These microfluidic solutions are based on various physical principles, such as mechanical trapping, electrical trapping or optical trapping. The most common principles applied in microsystems are further explained below and also some advantages and disadvantages of these approaches are mentioned when they are to be applied specifically for parallel SCA.

Mechanical trapping
With the use of microfabricated structures it is possible develop a platform that allows manipulation and trapping of cells. Effective functionality can be achieved with low fabrication complexity and it is an inexpensive solution when compared to the other trapping strategies. Although dynamic manipulation is possible, this approach is mostly chosen for passive trapping.

An example of an implementation with this approach is the use of laterally arranged trapping sites, implemented by creating an array of parallel side channels that are connected perpendicular to a main channel [5]. Single cells are trapped at the aperture of the side channel that faces the main channel by applying a pressure accross this aperture. This approach is easily scalable in order to achieve the parallel trapping of a large number of single cells and the process can be accomplished at a high speed by optimizing the trapping pressure and the flow rate of the cells. A disadvantage of this solution is that it is not a contactless method, which might result in damage inflicted to the cell membrane or irreversible attachment of the cells to the traps. Also, it is difficult to achieve high precision in cell manipulation, causing array sites to remain empty or leading to the accumulation of multiple cells in a trap [7].

Another mechanical approach is the use of planar aranged trapping sites, implemented by fabricating apertures in a two-dimensional microwell array [5]. With this method, very large amounts of cells can be processed in parallel. However, it will be more difficult to fabricate this compared to the lateral implementation, since every microwell needs to have an individual channel underneath it for transportation of the sample for analysis

When a non-contact manipulation force is needed, acoustic waves can be used. The principle is based on the phenomenon that an ultrasonic standing wave can generate a stationary pressure gradient, which will exert a force on the cell due to its different density and compressibility in relation to the liquid medium. This enables manipulation of cells with a trapping force in the range of hundreds of pN [6]. However, this approach is not compatible with the transportation of cellular compounds, since the drag force of the flow that emerges easily exceeds the trapping

force of the acoustic waves. Generally, this method is used for cell separation in agglomerates instead of manipulation of a single cell.

Electrical trapping
Electrical manipulation of cells in a LOC can be performed with electrophoresis or dielecrophoresis. Electrophoretic trapping utilizes the negative charge at the surface of the cells for manipulation in a DC electric field, while dielectrophoretic trapping is based on the dielectric properties of the cells relative to the buffer solution for manipulation in an AC electric field [5]. These methods are easy to apply and forces can be generated up to hundreds of pN [6]. Again, this principle is not compatible with transportation of cellular compounds, since the drag force of the flow that emerges easily exceeds the hundreds of pN trapping force of the electric fields. Also, electrodes are needed and their integration on microfluidic chips comes with a more elaborate, and therefore more expensive, fabrication process. The principle is easily scalable, a large number of electrodes can be placed in arrays for parallel trapping of the cells.

Optical trapping
With a focused laser beam, high precision manipulation of cells can be accomplished. The momentum that is carried by the Gaussian shaped profile of the laser beam can be transferred to the cell, causing it to be pulled to the center of the beam [6]. This offers a non-invasive manipulation method with high precision, but the throughput is low. Multiplexing can be accomplished with a prism, but the options for significant upscaling are limited and therefore this approach is not suitable for performing parallel trapping of many individual cells. Furthermore, the principle is not compatible with transportation of cellular compounds, since the drag force of the flow that emerges easily exceeds the pN trapping force of the laser beam that can be obtained.

Magnetic trapping
When cells are attached to magnetic beads, they can be trapped with the use of a magnetic field. When the particle is located in a magnetic field gradient, a magnetic force will act on it. Both permanent magnets and electromagnets can be used to generate the gradients. Traditionally, permanent magnets have been used because they can exert larger forces on the particles compared to electromagnets. The former can deliver tens of pN while the latter can exert a force that is typically a hundred times lower [6]. However, a system using electromagnets is more flexible and additional functionality can be added, such as using multiple poles that can more accurately move and rotate the bead/cell combination in the trap.

The disadvantage of the magnetic trapping approach is the fact that magnetic beads need to be attached to the cells, since the cells themselves exhibit no relevant magnetic properties. This will have an influence on the cell functioning and probably even its viability. Besided that, also this approach is not compatible with transportation of cell content, because the drag force of a flow will exceed the trapping forces. Moreover, this technology is currently mainly in use for the manipulation of large numbers of cells instead of single cell applications [5].

Table 2 summarizes the various cell trapping methods with their most important performance factors.

Table 2: Comparison of the available trapping methods on four important suitability factors.

Method	Implementation of the principle	Accurate control	Single living cell trapping and analysis	Scalability
Mechanical	+	-	+/-	+
Electrical	+/-	+/-	+/-	+
Optical	-	+	-	-
Magnetic	-	+/-	-	-

From these methods, the mechanical approach with lateral trapping structures is chosen for three main reasons. First, it is the easiest method to integrate on a chip. Only an external pressure controller is needed, no integrated electrodes are fabricated and therefore a relatively low amount of fabrication and operational costs are incurred. Second, this method is compatible with the transportation of cellular compounds, because the trapping force can exceed the drag forces of small flows. Third, it is easily scalable, so when the concept proves successful, the design can be modified for accomodation of a large number of cells for parallel analysis.

1.3.2 Cell membrane permeabilization

The second step that has to be completed is to gain access to the intracellular content of the trapped cells. Approaches for accessing the intracellular environment are basically classified as "destructive" or "non-destructive". With the destructive approach, the cell is lysed by damaging the membrane irreversibly to release the cellular content in the microsystem. If the cell has to proliferate, the membrane disruption should be transient. In this case, reversible permeabilization has to be used, creating pores that close either automatically or after application of an external stimulus.

Before comparing membrane permeabilization approaches, it is good to have a look at the structure of the cell membrane. The cell's plasma membrane is impermeable to most of the exogenous entities, preventing foreign entities such as drugs and particles from entering the cell. The membrane is based on amphipathic lipid molecules that are arranged in a bilayer. They have a polar head group that faces either the cells environment or the cytoplasm, and a nonpolar tail positioned in the bilayer interior. Figure 1 shows a picture of the basic structure of a cell membrane.

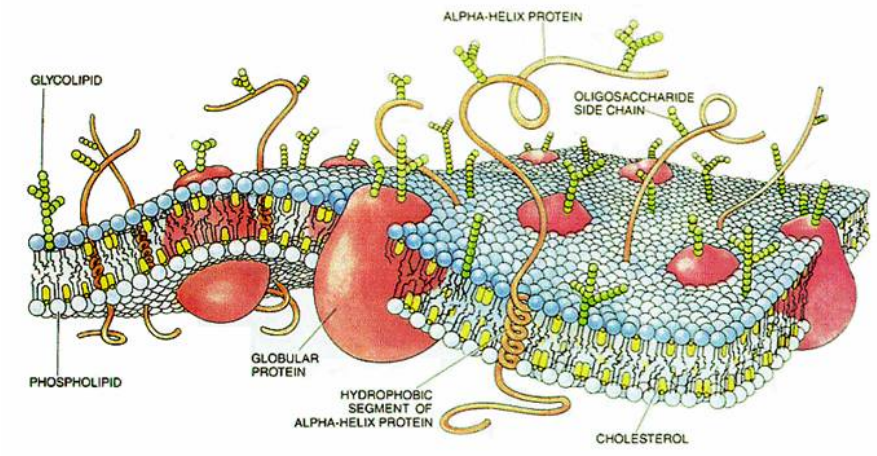

Figure 1: Schematic overview of the cell membrane, showing the basic structure and molecular content. The phospholipids are arranged in a bilayer that is reinforced with cholesterol. A variety of proteins that serve specific functions (transportation and communication) are inserted in or through the bilayer and glycolipids are inserted in the bilayer, facing the extracellular environment. Picture originates from www.ncnr.nist.gov.

The biomolecules that are most abundant in the membrane are phospholipids (in the form of glycerolipids or sphingolipids), cholesterol, glycolipids and membrane proteins [8]. Cholesterol is distributed almost equally in both of the monolayers and the amount can be up to 14% weight (30% mol) of the cell membrane. Membrane proteins can either be anchored in one monolayer or span the whole bilayer and they account for 50% of the weight of the cell membrane [9]. The mechanical properties of the membrane (stability and fluidity) are determined by its composition, which influences the packing density, the curvature of the bilayer and the molecular networking of the phospholipids [9, 10]. It is an important factor when the membrane is disrupted for sampling purposes, and of course its importance depends on the disruption approach that is chosen.

Different approaches can be used to gain access to the intracellular environment and these methods are all based on various chemical and physical principles. These are presented below, with an indication of their advantages and disadvantages if they are to be applied for parallel SCA.

Electrical permeabilization
The cell can be permeabilized by the application of an electrical pulse, or a train of pulses, accross the membrane to exceed its breakdown potential. The pulse length and amplitude determine whether the pores are transient, making the electroporation non-destructive, or whether the cell is lysed. These parameters are strongly cell-dependent [11].

The process of electroporation is fast, pores with a diameter of 0.5 to 400 nm are formed in the first milliseconds after application of the electric field and they close in seconds to minutes after removal of the electric field [9]. However, the successful formation of transient pores depends on a lot of factors, such as cell size and shape, and the membrane composition [11, 9]. This makes it a difficult procedure to control for a large number of single cells in parallel. Furthermore, electroporation on chip requires electrodes. Integration on the chip is mandatory for a reproducible elecric field, but it requires a complicated fabrication process. A more feasible and alternative approach relies on the introduction of external electrodes in the chip inlets.

Chemical permeabilization
The plasma membrane can be disrupted with various types of detergents, employing different mechanisms of membrane disruption. The chances of cell proliferation after the treatment are thereby affected in different ways. One method is to use detergents in the form of amphipathic molecules, having a structure similar to the phospholipid structure, that enter the membrane with their hydrocarbon chains. They act like 'wedges', putting pressure on the membrane and eventually breaking it. Another method is to use detergents which react with specific membrane components, forming complexes that disrupt the bilayer locally and thereby creating pores [12].

An example of the first method is the use of a dodecylsulphate salt (e.g. LiDS or SDS), which is an anionic detergent. Its structure is shown in figure 2

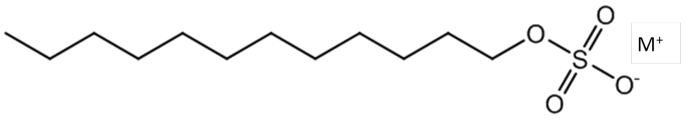

Figure 2: Structural formula of the dodecylsulphate salt that can be used for cell lysis. M^+ stands for Na^+ or Li^+.

When studying the effects of detergents such as DS^- salts on cell membranes, liposomes are often used as models for real cells. These studies show that the effects of different detergents as a function of the concentration that is used vary a lot among the available types of detergent [13]. At low concentrations, the molecules enter the lipid bilayer and as a consequence this bilayer changes its shape, becomes permeabilized and loses stability and at high concentrations, ultimately the whole membrane will be solubilized [14]. These effects take place within a couple of seconds [12]. Complete membrane solubilization is definitely a destructive approach, and no literature is found that describes a protocol for reversible permeabilization with detergents such as LiDS or SDS.

An implementation of the second method is the use of the nonionic detergent digitonin. When applied with the right protocol, digitonin can be used for reversible permeabilization of a cell membrane [15]. The structure of digitonin is shown in figure 3.

Digitonin forms a complex with cholesterol in the plasma membrane and when multiple of these cholesterol-digitonin complexes emerge, they combine into a membrane-spanning pore [16]. The presence of cholesterol is key to this permeabilization process and therefore membranes with a relatively high cholesterol content tend to be permeabilized easier. As a consequence it is thought that at low digitonin concentrations, the plasma membrane is permeabilized preferably

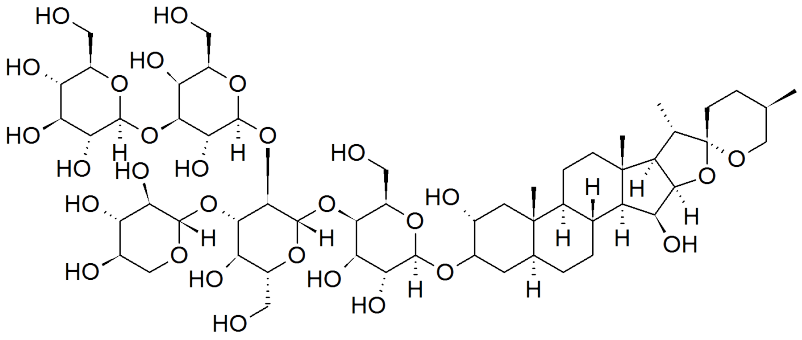

Figure 3: Structural formula of the nonionic detergent digitonin.

and not the the organelles that contain less cholesterol. This allows for selective permeabilization of different membranes based on their cholesterol content [16, 17]. The pores formed in the membrane are typically 8-10 nm in diameter, and their number depends on the membrane composition, the digitonin concentration and the exposure time to digitonin. Protocols are developed that use a digitonin concentration of a few micromolar and higher, exposing the cells for a couple of minutes and it is observed that these pores remain stable for several hours [16].

The permeabilization of the plasma membrane is reversible when digitonin is used at low concentrations. After permeabilization, the cells can be incubated in medium that is supplemented with a calcium salt, which helps resealing of the pores. No details are known about the mechanism of membrane resealing after digitonin treatment besides the idea that the presence of Ca^{2+} is involved, which is based on the fact that Ca^{2+} inhibits the permeabilization by digitonin [15].

The chemical permeabilization approach does not require additional equipment or complex integrated structures on the chips, keeping the microsystem fabrication easy and the operating procedure at a low cost. The chemicals can be delivered to the trapped cells by establishing a controlled flow, both in time and in space. Microfluidics enable this and standard methods are available, such as the use of syringe pumps (flow control), passive pumping (pressure control), or electroosmotic flow (EOF). These are investigated for their suitability.

Mechanical permeabilization

A variety of microfabricated structures can be used to cross the cell membrane. This approach can be implemented with sharp needles for the injection of well-defined amounts of liquids, providing non-destructive access to the cell's interior [5]. An advantage is that mechanical permeabilization does not depend on the membrane composition. The disadvantage is that complicated cleanroom fabrication steps are required for production of these needles. When polymer chips are used, the needles have to be produced separately and mounted into the chips afterwards. If the realization of the needles is compatible with the microchip fabrication, the method is more scalable, allowing the production of a many structures on a small surface area for the parallel processing of individual cells. However, this approach needs optical monitoring, making it difficult to scale up significantly.

Mechanical lysis can be done with the application of shear stress, by forcing the cell with a flow along a rough surface or centrifugation with spherical beads. This destructive method is easy to implement on a large scale on microchips and cells can be processed in parallel. However, the method is not suitable for single cells lysis, because the shear force causes mixing of the lysates from multiple cells.

Acoustical permeabilization

With sonoporation, pulsed ultrasonic acoustic waves are used for the creation of pores. The cell survival after permeabilization depends on the duty cycle of the acoustic waves and therefore it is possible to achieve non-destructive permeabilization [18]. However, this method is not optimal

for parallel permeabilization on chip, since acoustically transparent materials have to be used and the trapping structures disturb the focusing of the acoustic energy.

Optical permeabilization
Energy from a focused laser beam can be used to optoporate the plasma membrane. This is non-destructive if the energy of the laser light is limited [19]. Indirect optical permeabilization uses the energy of the laser to generate cavitation bubbles in the vicinity of the cell. These exploding bubbles can reversibly sonoporate the plasma membrane, enabling non-destructive permeabilization [20]. These two approaches are only suitable for permeabilizing a large number of single cells in parallel, if automatic focussing of the laser beam on its target can be accomplished automatically.

In table 3, a short feasibility assessment is provided for the on-chip application of the permeabilization methods described above.

Table 3: Summary of the feasibility of the on-chip permeabilization methods.

Method	Implementation of the principle	Reversible membrane poration	Parallel reversible poration of individual cells
Electrical	+/-	+/-	+/-
Chemical	+	+/-	+/-
Mechanical	+	+/-	-
Optical	+/-	+/-	-
Acoustical	-	-	-

The first column indicates how easy it is to implement the principle for permeabilizing a cell on a chip, so it gives the basic feasibility of applying the approach in general. The second column adds to this the constraint of reversibility and the third column shows the complexity that comes with scaling up the concept.

This table shows that both chemical and electrical permeabilization are attractive methods for non-destructive parallel permeabilization. They are relatively easy to implement on a microfluidic device and inexpensive. With electroporation, the optimal electric field strength and pulse length have to be found and when chemical permeabilization is used, the right concentration and exposure time have to be determined. In recent research efforts, the concept of electroporation is already studied in depth [9, 21]. Chemical permeabilization on chip is also studied, but to a lesser extent [16], and not within this research group. Therefore, it is at the moment interesting to further investigate the chemical permeabilization method.

1.3.3 Sampling out of the cells

The third step that has to be completed is the controlled sampling from the intracellular content and transporting this for analysis. When the membrane is disrupted, the cellular compounds are free to diffuse out of the cell (having a volume of 0.5 - 4 pL) into the microsystem channels (nL range). The concentration of a diffusive species will equilibrate to the extracellular concentration with a rate that is proportional to its concentration difference inside the cell and outside the cell. The equilibrium is established with an exponential dependence on the time, the pore size and the permeability of the plasma membrane [16].

When considering the detection, the dilution of the extractable sample from the cell needs to be minimized. Otherwise, the analysis of the biomolecules of interest is impossible due to the fact that its concentration will drop to undetectable levels. The sample to be analyzed needs to be confined in a small space at a concentration that resembles as closely as possible its original concentration in the cell.

A possible approach is transporting the biomolecules of interest in an electroosmotic flow (EOF) plug. When the cells are trapped and permeabilized, an electric field can be used to drag biomolecules out of the cell towards the analysis sites. The electric field has to be calibrated to

avoid cell lysis. A certain amount of dilution within the EOF plug is hard to avert. Keeping the cell compounds confined in a physically closed environment after cell permeabilization is the only way to avoid a high level of dilution and the mixing of content from different cells. Transporting the sample subsequently with an electric field provides a high level of control over the movement of the sample in time and space and therefore this approach is preferred.

1.3.4 Cell content analysis

The fourth step is the actual analysis of the biomolecules extracted out of the cell. The molecules of interest can be separated using capillary electrophoresis (CE) in the microchannel in which they are already transported [22], which is followed by detection.

Depending on the molecules to be detected, various other analysis principles are available. Proteins can be detected based on their selective hybridization with immobilized antibodies. For the analysis of mRNA and DNA which are present in small amounts, either an amplification step can be included or a sensor with single molecule detection capability can be employed. In the former, a reverse transcriptase polymerase chain reaction (RT-PCR) procedure is implemented on-chip and the subsequent detection of the produced cDNA copies can be done with an integrated microarray on which specific DNA probes are immobilized. Detection of DNA can be done with a similar process, with the difference that the reverse transcriptase step can be left out.

The binding of target molecules to the substrates can be detected electrically, raising opportunities for a high sensitivity. For example, the immobilization of the substrate could be done on nanowires, since these structures exhibit the promising sensitivity to perform the detection at the single molecule level. Furthermore, they can be realized using conventional microfabrication technology [23].

1.4 Summary of the parallel single cell analysis approach

The approaches that are chosen in this chapter for the implementation of the parallal single cell analysis functionality are summarized in table 4. These choices are made while considering complexity, cost and scalability, and only the aspects that are a topic in the remainder of this report are included.

Table 4: Implementation of parallel SCA functions on chip.

Analysis step	Implementation
Cell trapping	Mechanically (laterally arranged traps)
Cell permeabilization	Chemically (digitonin or LiDS) + Electrically
Cell content transportation	Electroosmotic flow

1.5 Project goals and preview

In the following chapters, the experiments and results will be described regarding this work on the parallel SCA platform. The following goals are set for this project:

1. Develop a microchip with a scalable design for controllable and reproducible trapping of individual living cells in parallel
2. Create pores in the plasma membrane of trapped cells
3. Investigate the possibilities to transport cellular content

In the next section of this report, the materials, equipment, protocols and procedures used in the experiments are presented. Subsequently, the chip design is described in more detail. Following this, the results of the experiments will be given with a discussion of these findings. This leads to a conclusion of the project and some ideas for future work on this topic.

2 Materials and methods

This chapter starts with an introduction to the chip design. Next, the mask fabrication process is described which is followed by the production of PDMS chips. Subsequently, protocols for cell culturing and cell staining are provided and finally the experimental setup and protocols for on-chip experimentation are introduced.

2.1 Chip design

The functionality that is to be implemented in the microsystem is introduced in chapter 1 (see table 4). Here, a conceptual description of the system will be given and more details are provided in chapter 3. This design is based on a system developed in previous work within BIOS in the frame of the collaboration with Oxford Gene Technology (OGT, www.ogt.co.uk).

Parallel analysis of a large number of cells is achieved using an array of structures for trapping and transportation of cell content. This allows a scalable approach for analyzing individual cells side by side. Figure 4 shows a conceptual illustration of the microsystem. It consists of a large main channel (red, 50 μm $\times$ 50 μm) and an array of small analysis channels (green, 10 μm $\times$ 10 μm) ending up in the main channel. The cells are loaded into the main channel and subsequently trapped with the help of an external pressure that is applied on the suction port (inlet B). After they have been trapped, the cells are permeabilized by loading a digitonin solution. Subsequently, the cellular content is extracted into the analysis channels using an electroosmotic flow (EOF) that is established between inlet A and B with external electrodes. For this transportation approach, the flow has to be created perpendicular to the main channel. Therefore, the identical network is designed on both sides of the main channel, together forming the side channel network.

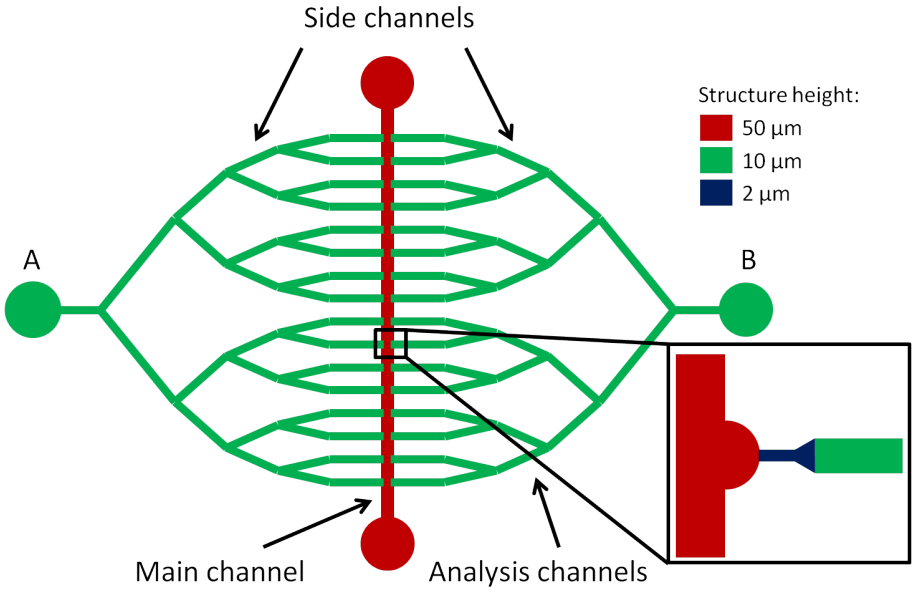

Figure 4: Conceptual design of the parallen SCA platform (not on scale). The dimensions of the system are 2 cm $\times$ 1 cm. Shown are the main channel (red, 50 μm $\times$ 50 μm) and the side channels (green, 10 μm $\times$ 10 μm). Inlet B is the suction port for cell trapping and the EOF for analyte transportation is established between inlet A and B. Inset: overview of one trap. Shown are the main channel with the trapping pocket, the trap constriction (blue, 4 μm $\times$ 2 μm), the transition structure (blue, 2 μm high) and the analysis channel (green, 10 μm $\times$10 μm).

The dedicated structure in which a cell is immobilized is shown in the inset of figure 4. It consists of a shallow trap constriction with an aperture in the main channel (4 μm $\times$ 2 μm). The aperture is located in a circularly shaped pocket (radius 10 μm) which can accomodate a single

cell. The microsystem contains 16 traps, allowing 16 individual cells to be trapped in parallel. Opposed to the main channel, the trap ends via the triangular shaped transition structure into the analysis channel. The layout of the analysis channel network is designed to ensure that an identical pressure is created accross every trap, so the length of the channel from inlet B to every trap is constant.

Three different structure heights are used in this design. Therefore, as explained in the next section, two alignment steps are included in the fabrication process. To create some room for mask alignment errors, the different layers overlap with at least 5 μm. This is shown in figure 5.

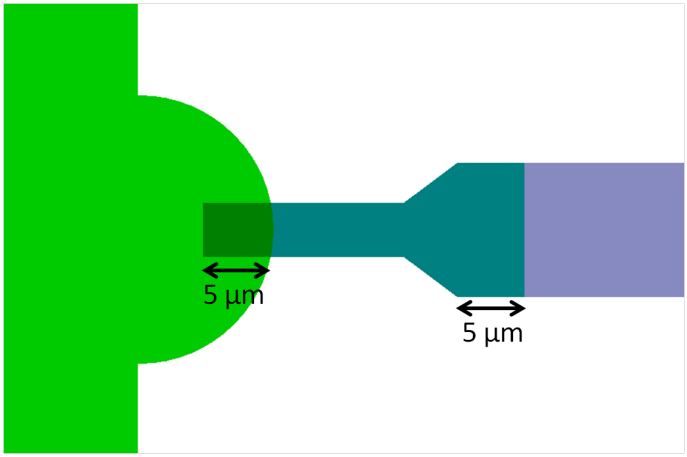

Figure 5: Picture of a trap, consisting of a trapping pocket (light green), constriction and transition structure (dark green). The analysis channel is shown in blue. Indicated is the 5 μm overlap between the three different layers that is chosen as a margin for the mask alignment.

2.2 Chip fabrication

This section describes the process steps that are involved in the chip fabrication. Chips are made from polydimethylsiloxane (PDMS) using soft lithography, which requires a mold for the repeated production of PDMS chips. The fabrication of the mold that is used in this process is explained first, followed by the production of PDMS chips.

2.2.1 Mold fabrication

The mold consists of a 4-inch silicon wafer, on which 3 layers of SU-8 (negative photoresist) are successively patterned using photolithography. After cleaning the wafer, 25 nm of aluminium is sputtered on the wafer which makes alignment possible due to its reflectivity. With this design, a proper alignment of the 3 layers of structures is crucial because the functionality of the traps depends on this. The design contains an overlap from the 50 μm layer to the 2 μm layer, and from the 2 μm layer to the 10 μm layer and every alignment has to occur within this margin (see figure 5).

SU-8 (5) is used for the 2 μm layer and SU-8 (50) for the 10 μm and 50 μm layers due to their difference in viscosity, allowing for production of respectively thinner layers (<5 μm) or thicker layers (>10 μm). The process of patterning is described for the first layer only.

2 μm SU-8 (5) is applied on the wafer by spin-coating. The photoresist is softbaked (95°C), after which the structures are patterned using photolithography. This is followed by a post-exposure bake (80°C) and subsequently the SU-8 is developed. The wafer is hardbaked (90°C) and finally the aluminium layer is etched with a standard procedure. Patterning of the two SU-8 (50) layers proceeds similarly.

As the Si wafer is brittle, increased risk of breaking exist when doing soft lithography. The Si wafer is secured on a thick glass substrate to increase the structural integrity of the mold. For that

purpose, the glass wafer is cleaned and provided with a layer of SU-8 (5) by spin-coating which will act as a glue. Subsequently, the SU-8 is softbaked and the Si wafer is attached to the glass substrate. Finally, the mold is hardbaked.

In order to ensure that the PDMS can be released from the mold when doing soft lithography, the mold wafers are coated with 1H,1H,2H,2H-perfluorodecyltrichlorosilane (FDTS) using a vapour-phase reaction in vacuum.

2.2.2 PDMS chip production

A solution is prepared from PDMS oligomers and a curing agent in a 10:1 mass ratio, which is mixed and degassed. The resulting PDMS mixture is poured over the mold that is secured in a custom made device. This allows control over the thickness of the PDMS and it ensures uniformity. The PDMS is degassed again, after which it is cured overnight at 60°C.

The cured PDMS layer is removed from the mold, the chips are cut using a sharp knife and the reservoir holes are punched with a sharp needle. Next, the chips are cleaned in isopropyl alcohol (IPA), together with the glass microscope slides on which they will be bonded. After drying, the PDMS chips and glass slides are activated using an oxygen plasma (400 mTorr) and subsequently the two components are assembled.

PDMS is intrinsically strongly hydrophobic and only after the oxygen plasma activation it is hydrophilic for approximately 1 day. However, there are a number of ways to maintain hydrophilicity for an extended period of time and two different methods have been tested here. The first consists of adding 0.5% - 0.7% of the non-ionic detergent Silwet L-77 Silicone copolymer to the PDMS base and curing agent mixture [24]. This detergent acts at the surface of the PDMS, keeping the chips permanently hydrophilic. The negative side effects are that the PDMS becomes brittle and it is hard to remove from the mold after curing. The second and preferred method is to store the chips directly after bonding in a (filtered) buffer solution until experiments are performed. Here, a 10 mM HEPES solution (10 mM HEPES, 140 mM NaCl, 2.68 mM KCl, 1.7 mM $MgCl_2$, 25 mM Glucose, pH 7.4) is used.

2.3 Cell culturing and staining

The procedure to maintain the cell culture is described, followed by the protocols for cell staining as a preparation for the on-chip cell experiments.

2.3.1 Cell culturing

P3x63Ag8 mouse myeloma cells are employed. These cells in suspension are cultured in Roswell Park Memorial Institute (RPMI) medium, supplemented with 10% Fetal Bovine Serum (FBS), 2 mM L-glutamine (LGL), 100 u/ml penicillin, 100 μg/ml streptomysin and 0.4 μg/ml Fungizone (final concentrations), giving RPMI+. The cell culture is stored in 25 cm^2 tissue culture flasks (T25 flask) in an incubator (37°C, 5% CO_2). Twice a week, the medium is refreshed and the cell suspension is diluted approximately 10 times. The cell concentration just before dilution is determined to be $\sim 10^6$ cells/ml, which is important for some of the cell staining protocols.

2.3.2 Cell staining

The cells are stained with the nuclear stain Hoechst 33342, an intercalating DNA dye, to visualize them. The dye is loaded with a final concentration of 1 μg/ml for a cell suspension in RPMI+ and incubated at 37°C for 20-30 min.

The viability marker calcein is a uniform stain. It is coupled to an acetoxymethyl group (AM), allowing transfer accross the cell membrane. Calcein starts to emit fluorescence after cleavage of the AM group by intracellular esterases. The creation of pores and cell lysis can now be visualized through the release of calcein from the cell. The dye is loaded with a final concentration of 1 μg/ml for a cell suspension in RPMI+ and incubated for 15-60 min at 37°C.

The lipophilic dye DiO stains the plasma membrane of the cell, allowing visualization of the membrane deformation that is induced by the trapping structures and the applied pressure. This dye is loaded with a final concentration of 5 μM for a cell suspension in serum-free medium (RPMI) and incubated for 15 min at 37°C.

Table 5 gives an overview of the different fluorescent dyes and their associated staining protocols.

Table 5: Summary of the available fluorescent dyes. Incubation is performed at 37°C and 5% CO_2.

Dye	Function	Staining concentration	Incubation time (min)
Hoechst	Permanent nuclear stain	1 μg/ml in RPMI+	20-30
Calcein	Viability stain	1 μg/ml in RPMI+	15-60
DiO	Plasma membrane stain	5 μM in in RPMI	15

Cells are most of the time stained with a combination of calcein and Hoechst. In this case, cells are incubated for 30 min and subsequently washed 2× and stored in 10 mM HEPES. Besides looking at the release of calcein, the cell membrane permeabilization is visualized using the entry of the membrane integrity stain propidium iodide (PI), which stains the DNA in the cell when the membrane is damaged. This allows for a more accurate estimation of the permeabilization time because calcein suffers from fast photobleaching.

The wavelengths of maximum excitation ($\lambda_{ex,max}$) and emission ($\lambda_{em,max}$) of the fluorescent dyes that are used for on-chip experimentation are summarized in table 6. Also the specifications of the laser and the emission filters of the microscope that fit best with these wavelengths are mentioned.

Table 6: Excitation and emission wavelengths of the fluorescent dyes that are used for cell staining. The excitation filter is of the bandpass (bp) type and the center wavelength with the full width at half maximum (FWHM) is given. The emission filter is of the long pass (lp) type and the cut-off wavelength is given.

Dye	$\lambda_{ex,max}$ (nm)	$\lambda_{em,max}$ (nm)	Excitation filter (nm)	Emission filter (nm)
Hoechst 33342	350	461	335 bp 70	400 lp
Calcein AM	494	514	455 bp 70	510 lp
DiO	484	501	455 bp 70	510 lp
PI	535	617	470 bp 40	520 lp

2.4 Fluidic protocols in the microfluidic system

Handling of cells and chemicals on the chip requires accurate control over the flows through the channels. For the various steps in parallel SCA, different types of liquid handling is suitable. The cells are loaded with passive pumping. Buffers and the permeabilization solution are introduced using a pressure driven flow (PDF). The cell content is subsequently transported with an electroosmotic flow (EOF). These 3 principles are explained in more detail.

2.4.1 Pressure driven flow

The use of a syringe pump is an easy method to control the flow velocity in a microchannel. However, this flow turns out to be unstable due to the flexible tubing and the stepper motor in the pumping equipment, especially when low flow rates are employed. Still, this method is preferred for simple loading of chemicals, such as a buffer or digitonin, where a low and precise flow rate is not required. Since various substances have to be introduced in the channel, these are placed in droplets on the inlets and subsequently introduced in the channel by suction with the syringe pump.

2.4.2 Passive pumping

The passive pumping method is based on the phenomenon that drops of different sizes exhibit a different internal pressure. The pressure difference at the liquid-air interface of a spherical drop with radius R and surface tension γ is described by the Young-Laplace equation [25]:

$$\Delta P = \frac{2\gamma}{R} \tag{1}$$

This pressure difference is inversely proportional to the radius of the droplet. When a droplet of radius R_1 (inlet drop) is placed on a reservoir and a droplet of radius R_2 (outlet drop) is placed on another reservoir ($R_1 < R_2$) and both are connected with a microchannel, the pressure difference accross this channel is reported in [25]:

$$\Delta P = 2\gamma(\frac{1}{R_1} - \frac{1}{R_2}) \tag{2}$$

This ΔP will result in a flow through the microchannel from the inlet to the outlet. The flow rate will decrease with decreasing volume of the inlet drop and can be increased with replenishment of the input drop when the flow starts to cease. The flow rate therefore shows a sawtooth behaviour in time, but it is smooth (i.e. there is no high frequency pulsation), also at very low flow rates. These properties make this method attractive for the cell loading. Finally, it is a promising pumping method in general when microfluidics is to be used in large scale industry applications, because the only equipment needed to establish the flow is a droplet dispenser such as a standard liquid handling robot.

2.4.3 Electroosmotic flow

The electroosmotic flow (EOF) is based on the phenomenon that the movement of certain liquids in a channel can be established by applying an electric field accross the channel. This electric field initiates movement of the ions in the channel and these ions drag the liquid along with it. A more detailed description of the EOF is given in chapter 3.

EOF allows an accurate control over the liquid movement in time and space. For the flow control, electrodes are introduced in the chip reservoirs. The flow is established instantaneously upon application of the electric field and it is immediately stabilized, also at very low flow rates. The disadvantage is that the behaviour of the flow depends on the surface charge of the PDMS channel, the viscosity of the buffer and the conductivity of the buffer which are not always constant. Furthermore, to obtain a uniform and stable EOF plug, the hydrodynamic forces in the chip should be entirely suppressed, which is very difficult to achieve.

However, the level of control that is needed for the transportation of cellular content into the analysis channels can be achieved in principle with this concept and not with the other liquid handling methods. Therefore, it is the most promising liquid handling technique for this application.

2.5 Experimental setup

The complete experimental setup can be seen in figure 6. It comprises a microscope for visualization of the experiments, a Maesflo pressure controller, a syringe pump and an EOF voltage source. These components are detailed below.

Cell trapping is performed with a pressure source (Maesflo) that is connected with the suction port on the chip. This system consists of a four channel Microfluidic Flow Control System (MFCS) and a flow meter (Flowell). The MFCS is capable of controlling the pressure in the range of 0 to -345 mbar with a precision of 0.1% of the full scale (0.0345 mbar). An external pressure source is connected to the MFCS, providing -780 mbar input pressure. If the flow rate is measured with the Maesflo system after loading the cells into the main channel, it is possible to determine through the change in flow rate when a cell is trapped. The chip design consists of 16 traps, which are

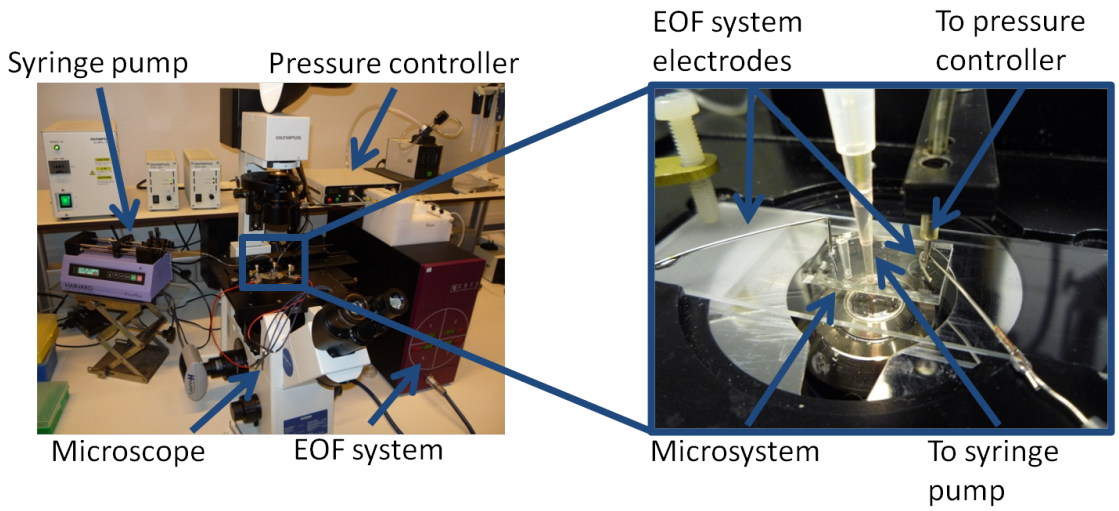

Figure 6: Overview of the experimental setup consisting of the microscope, EOF voltage source, syringe pump and Maesflo system. Inset: chip that is mounted on the microscope stage. Indicated are the various connectors to the equipment. The inlet of the main channel that is not used is sealed using a shortened pipette tip that is previously closed with heat treatment.

initially assumed to be all open. The flow rate that follows from the applied pressure will decrease when a trap is blocked with a cell. This decrease is 1/16 of the initial flow rate when the first cell is trapped, 1/15 of the remaining flow rate when the second cell is trapped and so on. This is, besides optical inspection with the microscope, a detection system for cell trapping. It will become a useful tool when the system is scaled up to the order of magnitude of e.g. 1000 cells, which is needed to become statistically relevant. Optical inspection will be more difficult in this situation and the fluidic detection method can be adapted for automation of the cell trapping procedure when large scale parallellization is implemented.

Flushing the channels with buffer and introducing the digitonin for membrane permeabilization is done with a syringe pump using a 100 μl syringe that is connected to the main channel. The flow rate is set to 2 μl/min.

Transportation of the cell content is performed with an electroosmotic flow (EOF). The voltage source (IBIS μfluidics) provides a potential up to 1000 V and gives real-time readings of the applied potential and the measured current. It is connected to the inlets of the side networks with Pt electrodes. The experiments on the chip are followed optically using an inverted microscope equipped with a mercury burner for the fluorescence spectroscopy and two lamps for bright field images, allowing illumination from the top and the bottom. A computer is used to control the Maesflo and EOF equipment with dedicated LabView software. The camera attached to the microscope is controlled with dedicated Olympus Soft Imaging Solutions software.

2.5.1 Experimental protocols

The chip is mounted on the microscope stage and the reservoirs are connected to the equipment as follows (reservoir numbers can be found in figure 7 in chapter 3). The pressure controller is connected to inlet 8, the syringe pump to inlet 2 and EOF electrodes are introduced in inlets 6 and 8. Inlet 1 is closed and inlets 5 and 7 are left open, because their influence on the flow in the main channel is expected to be neglectible due to the small dimensions of the side channels.

The chips are prepared by incubating a filtered solution of 5% BSA in 10 mM HEPES in the channels for 2 h, to avoid sticking of the cells to the channel surfaces during the experiments.

The calcein and Hoechst stained cells are loaded with passive pumping. This flow is initiated by placing 15 μl of HEPES on inlet 4 and 1.5 μl of cell suspension on inlet 3. The cells will flow

through the main channel at a speed of 100 - 200 μm/s. It typically takes 30 s to 2 min for the cells to move through the inlet and to enter the main channel.

As soon as the cells enter the main channel, the pressure controller is activated at -30 mbar to trap the cells. When all the functional traps are filled with a cell, the pressure is reduced to -10 mbar in order to reduce the stress on the cell membranes. It is possible that traps accomodate more than one cell. In the experiments, only the traps with a single cell will be followed.

A 5 μl droplet of 10 μg/ml digitonin in a Ca^{+2}-free solution of 10 mM HEPES supplemented with 10 μg/ml PI is placed on both inlets 3 and 4 and this is flushed with 2 μl/min for 1 min (if the intention is to reseal the membrane, PI is left out). Subsequently, the pressure is switched to 0 mBar and the cells are incubated in the digitonin solution until PI entry is observed. A picture is taken every second using the 520 nm lp filter for PI detection.

When the membrane is permeabilized, the cellular content diffuses into the main channel, visualized in the form of calcein diffusion. This is transported into the side channels by establishing an EOF accross the side networks. Various driving voltages are tested for this purpose: 50, 100, 200 and 500 V.

3 Chip design

In this chapter, the microchip that is designed for the SCA experiments is discussed. First, the design choices concerning the microstructures are explained. These parameters are subsequently used to calculate the pressure drop over the trap as a function of the input pressure from the Maesflo. Next, the design parameters are used to develop a model for the EOF as a function of the driving voltage accross the side networks.

The mask is designed in CleWin and the chip layout is shown in figure 7. The 4 inch silicon mold accomodates 18 chips of 2 cm $\times$ 1.2 cm. This enables to easily vary a number of feature sizes in the design and to study their influence.

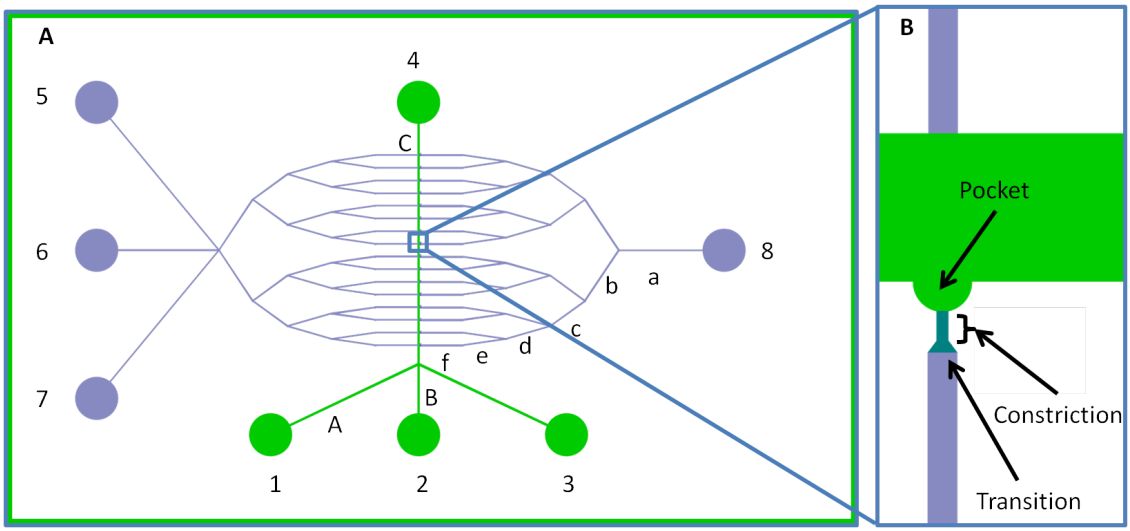

Figure 7: Chip layout as developed in CleWin. A: overview of the chip layout. Inlet 8 is connected to the Maesflo pressure controller for cell trapping, the EOF is established between inlets 6 and 8, the cells are loaded in inlet 3 and the flow for introducing the permeabilization solution is established from inlet 2. B: enlargement of a trap.

The design contains 6 variations of the chip. The length of the trap constricion is varied as well as the width of the main channel. Table 7 lists the parameters of the designs.

Table 7: Dimensions of the structures on the chip.

Structure	Dimension (μm)
Main channel width	500 and 100
Main channel height	50
Side channel width	10
Side channel height	10
Trap constriction length	0, 4, 10 and 30
Trap constriction width	4
Trap constriction height	2
Transition structure length	4
Transition structure height	2
Trapping pocket radius	10
Channel length inlet 1 - inlet 4	9060
Channel length inlet 2 - inlet 4	6870
Distance inlet 5 - main channel	9645
Distance inlet 6 - main channel	7995
Distance transition - inlet 8	7585

The diameter of a P3x65Ag8 cell is on average 15 μm and this is taken into account when choosing the dimensions of the structures. The main channel has a cross section of 50 μm $\times$ 50 μm. On one hand, this is big enough to suppress clogging issues, and on the other hand, it limits the distance cells have to travel to reach the trap. A width of 100 μm is also used on a few chips to test this latter hypothesis.

The dimensions of the traps are chosen as to accommodate a single P3x65Ag8 cell while limiting the risks for multiple cell trapping. The pocket is 20 μm in diameter and the trapping constriction is 2 μm in height and 4 μm in width. These dimensions are used in previous work in the BIOS group carried out in collaboration with OGT and they had shown to work for cell trapping. A 3 μm constriction height allowed the living cells to move through the constriction, while a 2 μm constriction height causes the cells to be retained in the pocket.

The membranes of living cells exhibit a varying degree of rigidity. As a consequence, the cell can be trapped in two different modes when the trapping pressure is applied to the analysis network, as is shown in figure 8. In mode 1, the cell is trapped in front of the aperture of the trapping constriction, maintaining its spherical shape. In mode 2, the cell is squeezed into the trap constriction, stretching the membrane. These two different modes have shown to play an important role in the cell permeabilization and sampling procedures.

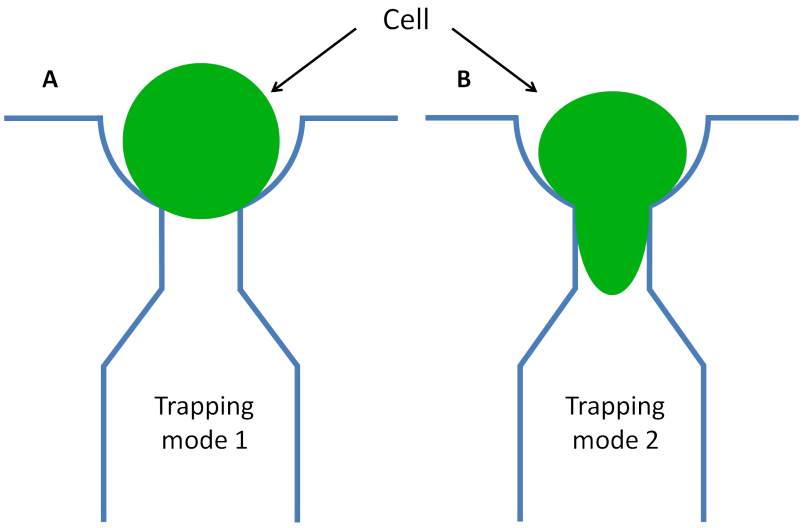

Figure 8: Illustration of cell behaviour in a trap. A: cell is trapped in the pocket, in front of the constriction. B: cell is squeezed in the trap constriction. These different trapping modes are thought to be the result of varying membrane rigidity.

Figure 9 shows a 3D impression of the chip design (view from the bottom), showing the configuration of the main channel, the side channels and the traps on scale.

The various lengths of the trap constrictions are 0, 4, 10 and 30 μm, comparable with 0 - 2 cell diameters, allowing the study of the dependancy of the trapping success on the constriction length in a relevant range.

The trapping pressure is applied to the traps via the analysis channels using equipment that generates a limited pressure range. To find the optimal pressure for cell trapping, the pressure range that is actually applied over the traps should be as large as possible to allow variation, meaning that the hydrodynamic resistance of the analysis channels has to be low. Side channel cross-sectional dimensions of 10 μm $\times$ 10 μm are considered suitable, because the resistance is limited and simultaneously it is sufficiently small, preventing the cells from entering the side channels and making visualization of released cell content possible. The resistance also depends on the length of the channel, but this length is already determined through the equal distribution of the inlets over the chip surface. Moreover, the resistance depends linearly on the length, while the channel height and width exhibit a higher impact.

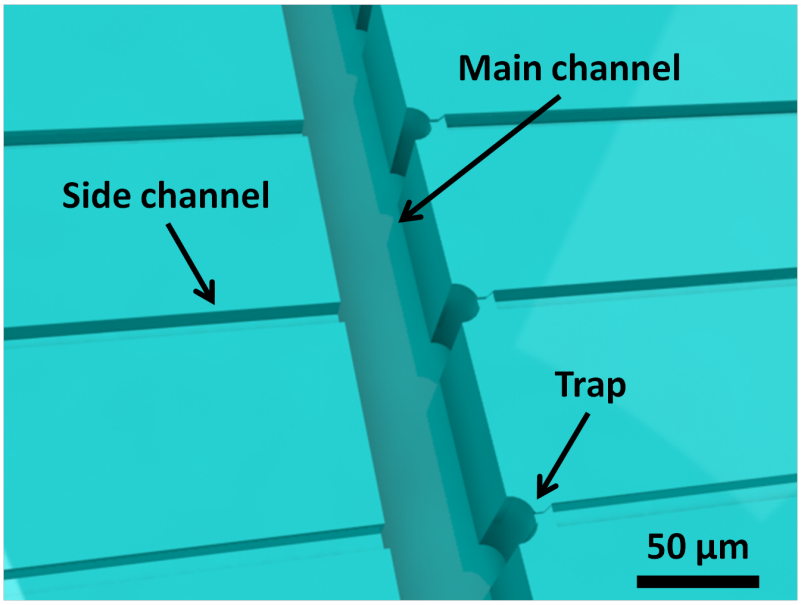

Figure 9: 3D impression of the chip configuration consisting of the traps, the main channel and the side channels. This is a view from the bottom and the dimensions are on scale.

3.1 Pressure driven flow

A channel section has a hydrodynamic resistance R_h, which is defined as the ratio of the pressure difference (ΔP) accross the channel and volumetric flow rate (Q) through the channel:

$$R_h = \frac{\Delta P}{Q} \tag{3}$$

In which

$$\Delta P = -\frac{\partial P}{\partial x} l \tag{4}$$

Figure 10 indicates these parameters ($\Delta P = P_{high} - P_{low}$).

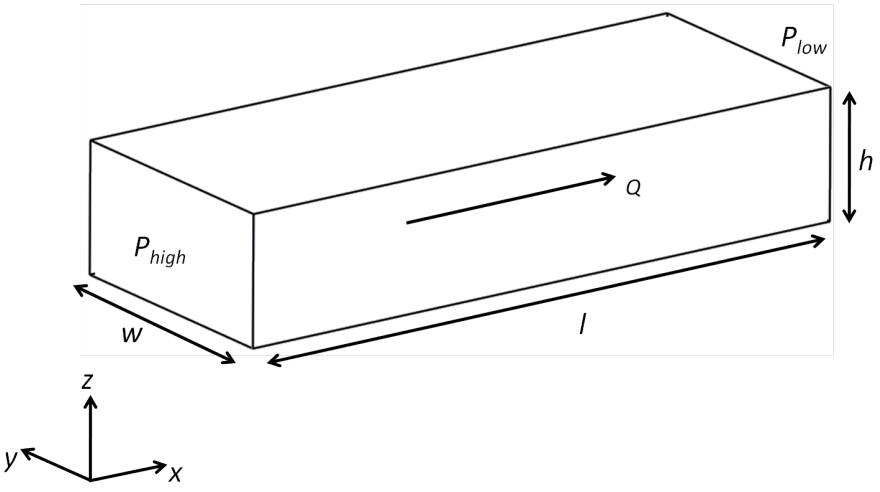

Figure 10: Fluidic channel section (dimensions l, w and h) with a pressure difference $\Delta P = P_{high} - P_{low}$ and a volumetric flow rate Q.

The pressure acts solely in the x-direction, resulting in a flow in the x-direction only which is laminar and fully developed. The flow velocity profile in y and z is described by the Poisson equation:

$$\frac{\partial^2 u_x}{\partial y^2} + \frac{\partial^2 u_x}{\partial z^2} = \frac{1}{\eta}\frac{\partial P}{\partial x} \tag{5}$$

The following boundary conditions are employed:

$$\begin{aligned} \frac{\partial u_x}{\partial y} &= 0 \qquad y = 0 \\ u_x &= 0 \qquad y = w \\ \frac{\partial u_x}{\partial z} &= 0 \qquad z = 0 \\ u_x &= 0 \qquad z = h \end{aligned}$$

This equation is solved for $u_x(y,z)$ in the work of [26]. The volumetric flow velocity is obtained by integration of $u_x(y,z)$ over the cross-section of the channel (width and height) and subsequently equation 3 is used to find R_h. These calculations are reproduced in appendix A. Finally, the following conditional approximation for R_h is used [27]:

$$R_h \approx \frac{12\eta l}{h^3(w - 0.63h)} \qquad w \geq h \tag{6}$$

Maple is used to plot R_h as a function of the channel width, using a viscosity of η = 0.75 mPa·s for HEPES and for the side channel a total length of 7585 μm and a height of 10 μm. Figure 11 shows the resulting plot.

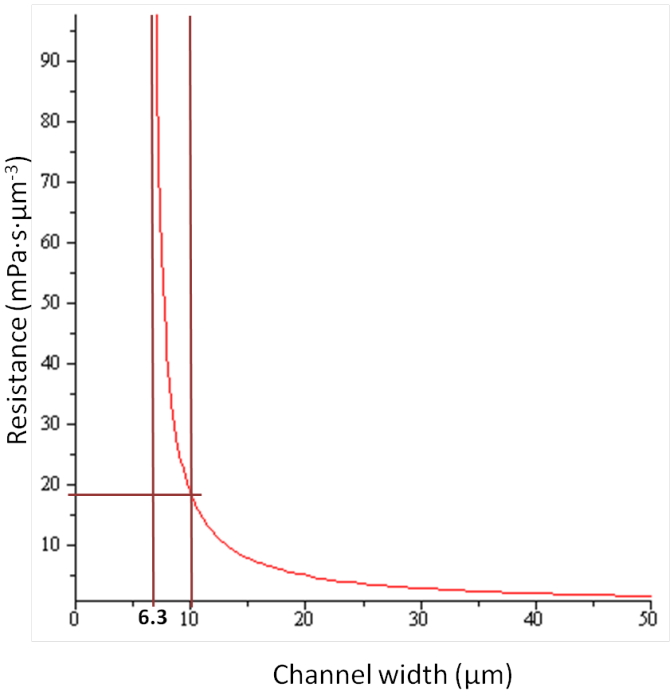

Figure 11: Hydrodynamic channel resistance dependency on the channel width of a 7585 μm long, 10 μm high side channel filled with HEPES (η = 0.75 mPa·s).

This graph shows a rapid decrease of the channel resistance as a function of the channel width, above the asymptotic value of 6.3 μm from this approximation. In the design, the channel width is

Table 8: Length and resistance of different channel structures. See figure 7 for their arrangement in the chip layout.

Channel structure	Length (μm)	Resistance (mPa·s·μm^{-3})
Tubing	$1 \cdot 10^6$	$7.8 \cdot 10^{-3}$
a	1990	4.84
b	1440	3.50
c	1025	2.49
d	1090	2.65
e	1040	2.53
f	1000	2.43
Transition structure	4	0.78
Trap constriction	0	0
Trap constriction	4	1.64
Trap constriction	10	4.11
Trap constriction	30	12.3
A	3340	$1.30 \cdot 10^{-2}$
B	1150	$4.48 \cdot 10^{-3}$
C	5720	$2.23 \cdot 10^{-2}$

chosen to be 10 μm, providing a resistance of 18.45 mPa·s·μm^{-3}. This is a good trade-off between a small resistance and a practical size for fluorescence microscopy.

In this design, 16 traps are incorporated. This is an amount low enough to track the cell trapping manually, but still large enough to show the large-scale capability and the possible automation of the cell trapping process. The layout of the analysis channels is chosen to have an equal channel length between every trap and inlet 8, making sure that the pressure drop accross every trap is identical. The channel inlets are 1 mm in diameter and spaced at least 2.5 mm apart from each other. This is needed for the application of individual droplets on the inlets when liquids are introduced with either passive pumping or suction using the syringe pump.

The resistance of both the channel structures and the tubing that connects the pump to inlet 8 is calculated to determine the pressure applied accross the trap constriction for cell capturing. The resistance of the tubing can be calculated with equation 7, which follows from the standard solution of the Navier-Stokes equation for a flow profile in a circular tube:

$$R_{hy} = \frac{8\eta l}{\pi a^4} \tag{7}$$

with a the radius and l the length of the tubing and η the viscosity of HEPES. The resistance of this tubing and the channel structures are summarized in table 8.

The network of analysis channels is built up in 'levels' and every level contains the double amount of channel structures having equal length. In figure 7 these structures are indicated with a letter (a-f) and in table 8 these lengths can be found with their corresponding resistance. The transition structure, connecting the trap to the analysis channel, is approximated by a rectangular structure of 7 μm in width, which is the mean value of the actual width of the structure.

For the determination of the pressure drop over the traps, the approximation is made that the resistance in the main channel has such a small value compared to the resistance in the analysis channels and the traps, that the pressure at the location of every trapping pocket can be considered the same and neglectible. This is needed because otherwise four extra and unequal resistances in the direction of the outlets will appear at every trapping pocket. The largest error that is made with this approximation occurs at the trapping pocket in the middle of the main channel and is smaller than half the main channel resistance, which is < 0.018 mPa·s·μm^{-3} (0.23% of the side network resistance). Therefore, this contribution to the total resistance is ignored. Also, the variation in the length of channel piece 'f' that arises due to the varying length of the trap constriction is not taken into account (see table 8). The error that arises by neglecting its contribution is at

Table 9: Pressure drop accross the 4 different types of trap. The input pressure applied on inlet 8 is -30 mbar.

Trap length	Pressure drop (mbar)	Volumetric flow rate ($\mu\mathbf{m}^3 \cdot \mathbf{s}^{-1}$)	Hydrodynamic power (fW)
0	-2.71	-3.47	0.94
4	-7.06	-2.92	2.06
10	-11.5	-2.35	2.70
30	-18.8	-1.44	2.68

most 0.06% of the total resistance. The total resistance of the side network, from inlet 8 towards the trap, can now be calculated with the values of table 8:

$$R_{side} = R_{Tubing} + R_a + \frac{R_b}{2} + \frac{R_c}{4} + \frac{R_d}{8} + \frac{R_e}{16} + \frac{R_f}{16} \tag{8}$$

This results in a R_{side} of 7.86 mPa·s·μm^{-3}.

The combination of the trap constriction and the transition structure together form R_{tr}, which is either 0.78, 2.42, 4.89 or 13.10 mPa·s·μm^{-3}, depending on the length of the trap constriction (respectively 0, 4, 10 or 30 μm).

The pressure drop P_{tr} over the trap follows from the input pressure that is applied at inlet 8 and a resistance divider with the side channels and the trap:

$$P_{tr} = \frac{R_{tr}}{R_{tr} + R_{side}} \cdot P_{in} \tag{9}$$

Table 9 lists the pressure drop accross the various traps when the input pressure is set to -30 mbar. The flow rate is calculated with equation 3 and the hydrodynamic power (HP) can be obtained with:

$$HP = \frac{Q \cdot \Delta P}{10} \tag{10}$$

Figure 12 gives a plot of the power dependency on the constriction length, showing that a length of 17 μm would provide the largest power. Therefore, the 10 μm constriction is expected to provide the largest power from the various designs available.

3.2 Electroosmotic flow

The voltage driven electroosmotic flow (EOF) is employed widely in microfluidics for accurate manipulation of liquid samples. The method relies on the surface effects of the channels in the system (see figure 13) and microchannels exhibit a high surface-to-volume ratio. The surface of a glass or PDMS wall is negatively charged and the electrical double layer (EDL) near the wall contains a positive net charge in the form of accumulated ions from the electrolyte buffer solution. The applied electric field over the full length of the channel exerts a force on these ions, causing them to move towards the cathode while dragging the liquid in the channel along by viscous coupling. This mechanism produces a flat flow profile, in contrast to the parabolic flow profile of a pressure driven flow and it is possible to establish well-controlled flows at low flow rates.

The EDL follows from the surface potential of the channel material, which is caused by SiO^- groups in glass channels and OH^- groups in PDMS channels [28]. This negative surface charge results in a layer of positive ions against the channel wall (Stern layer), giving a ζ-potential of -66 to -88 mV for glass and -68 and -110 mV for PDMS [29]. The Stern layer attracts positive ions from the electrolyte solution in the diffuse layer, giving a net positive charge. The EOF is established when the E-field exerts a force on these mobile ions. The flow velocity v_{eof} depends linearly on the driving voltage:

$$v_{eof} = \mu_{eof} E \tag{11}$$

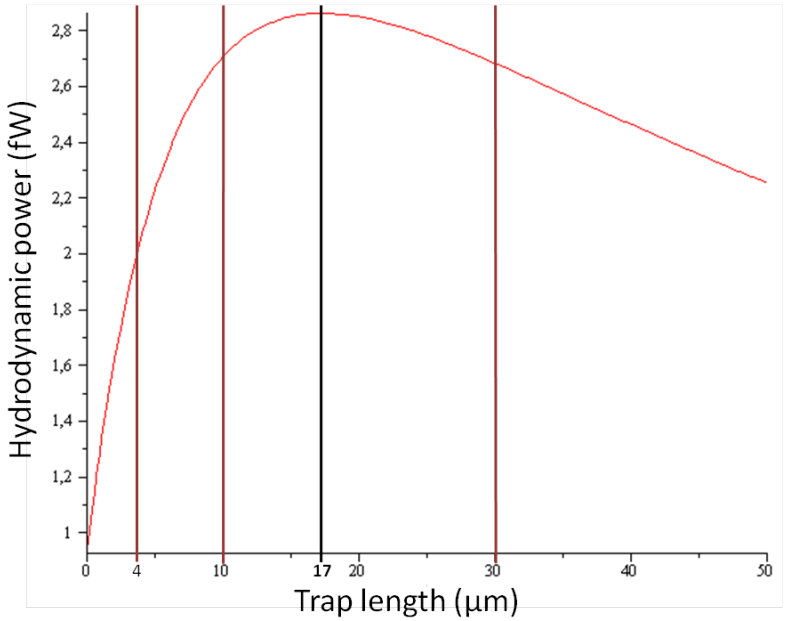

Figure 12: Hydrodynamic power provided by the traps as a function of the trap length.

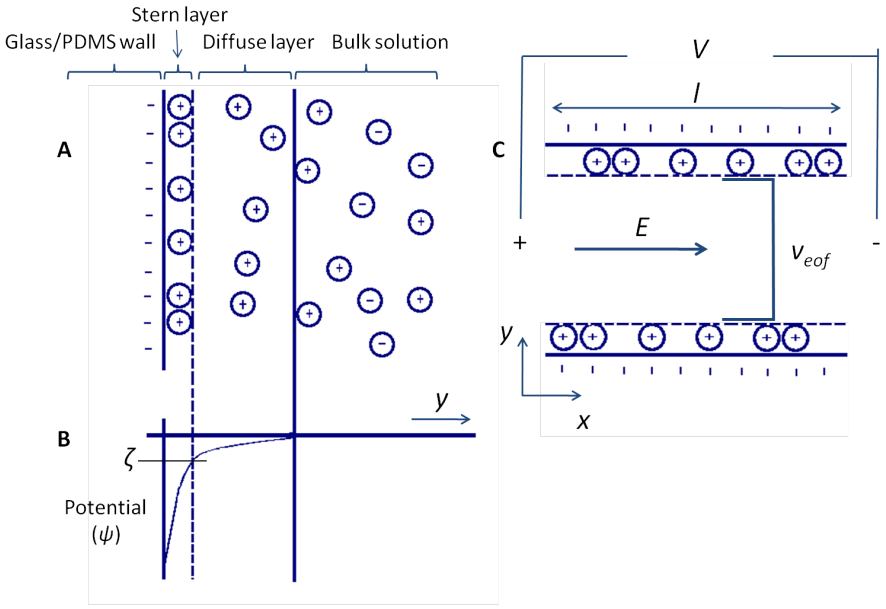

Figure 13: Surface effects of the channel wall are exploited for the establishment of an EOF. A: development of an electrical double layer (EDL) near the channel wall as a result of the negative surface charge. B: potential distribution in the EDL, with the ζ-potential at the Stern layer. C: establishment of an EOF upon application of an electic field, providing a plug flow.

with μ_{eof} the electroosmotic mobility, which depends on the ζ-potential, the relative permittivity of the buffer (ϵ_r) and the dynamic viscosity of the buffer (η) according to the Smoluchowski equation:

$$\mu_{eof} = -\frac{\epsilon_0 \epsilon_r \zeta}{\eta} \tag{12}$$

The volumetric flow velocity (Q) in μL/min is:

$$Q = v_{eof} A = \frac{\mu_{eof} V_0}{l} \cdot 6 \cdot 10^{-8} \tag{13}$$

with V_0 the applied voltage, l the length of the channel and A the cross-sectional surface area. The geometric dimensions are in μm.

The current through the channels (I_{eof}) can be measured to characterize the established EOF:

$$I_{eof} = \frac{V}{R_{el}} = \frac{V_0 \cdot A}{\rho \cdot l} \tag{14}$$

with R_{el} the electrical resistance of the channel and ρ the resistivity of the buffer.

The flow rate and the current in the analysis channels are calculated using relevant material parameters for PDMS and 10 mM HEPES. Since a channel contains three PDMS walls and one glass wall, it is assumed that the PDMS surfaces will be dominant and therefore a μ_{eof} of $7.4 \cdot 10^{-8}$ $m^2 \cdot V^{-1} \cdot s^{-1}$ for PDMS is used [30]. Furthermore, a resistivity of $6.21 \cdot 10^3$ $\Omega \cdot \mu$m for 10 mM HEPES buffer is determined.

When the EOF potential is applied between inlets 6 and 8, three distinct resistances appear in the EOF network, due to the side channels after inlet 6, the trap and the analysis channels (see figure 14). The voltage drop accross the main channel is neglected in the calculation of the flow rate, which introduces an error of 0.2% on the total resistance of the side networks.

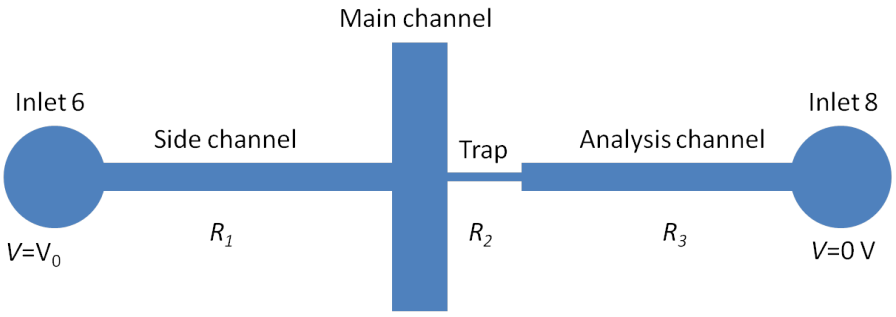

Figure 14: Schematic drawing of the channel structure as employed for the EOF establishment. It is subdivided in 3 basic structures (with resistance R_1, R_2 and R_3) that contain 3 corresponding voltage drops that drive the flow.

The flow rates and the electric fields generated using various values of V_0 can be found in figure 15 for the analysis channel and the trap. In the model, the trap consists of a rectangular structure having the width and height of the constriction and a length corresponding to the sum of the constriction and the transition structure.

The voltage drop accross the analysis channel is:

$$V_1 = \frac{R_3}{R_1 + R_2 + R_3} \cdot V_0 \tag{15}$$

and the voltage drops accross the other segments can be calculated in a similar way. The variation in the voltage drop accross the analysis channel when the constriction length is varied, is neglected. The electric field in the constriction does not depend significantly on its own length since its resistance scales linearly with its length, but due to the resistance divider (equation 15) a small variation is introduced. The electric field is enhanced 12.5 times in the constriction due to the difference in surface area between the trap and the analysis channel, which are 8 μm^2 and 100 μm^2 , respectively. The flow rate is therefore 12.5 times higher in the trap, while the total volumetric flow rate in the system remains equal in both structures.

With the establishment of an EOF, a risk for cell lysis exists due to the enhancement of the electric field in the traps. For cell lysis, the critical transmembrane breakdown potential has to be exceeded. Generally, the membrane breakdown potential is around 1 V, which is accomplished

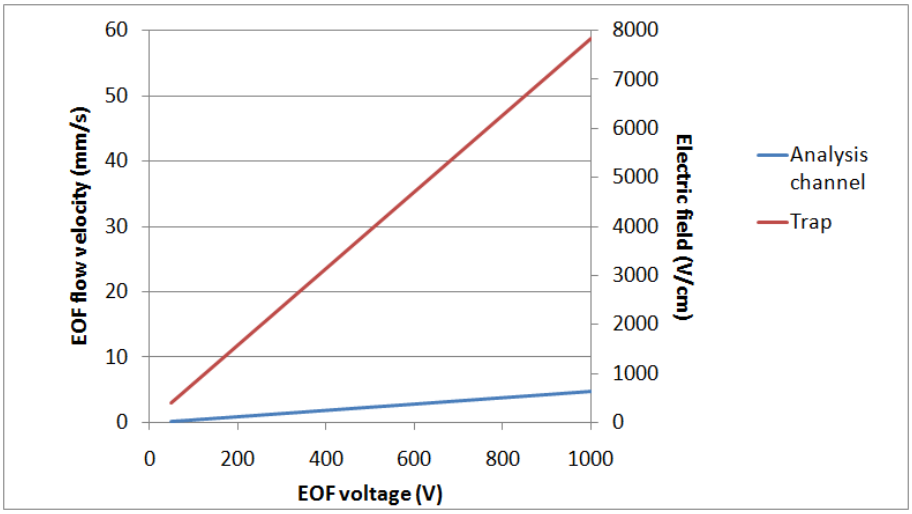

Figure 15: Flow velocity and electric field in the analysis channels and traps as a result of the applied voltage. The dependency of the flow rate and field on the trap constriction length is not significant and therefore this model can be used for the 4 types of the chip available.

with an electric field in the low kV/cm range [11]. Therefore, the maximum EOF driving voltage that can be used is 100 V to avoid cell lysis, providing an EOF flow rate of 0.47 mm/s in the analysis channels.

The established flow is characterized by a current measurement (see equation 14). The total resistance of the side channel networks follows from equation 8, when it is supplemented with the trap structures and the opposite side network. The current as a function of the driving voltage can be obtained from the application of Ohm's law and this relation is plotted in figure 16.

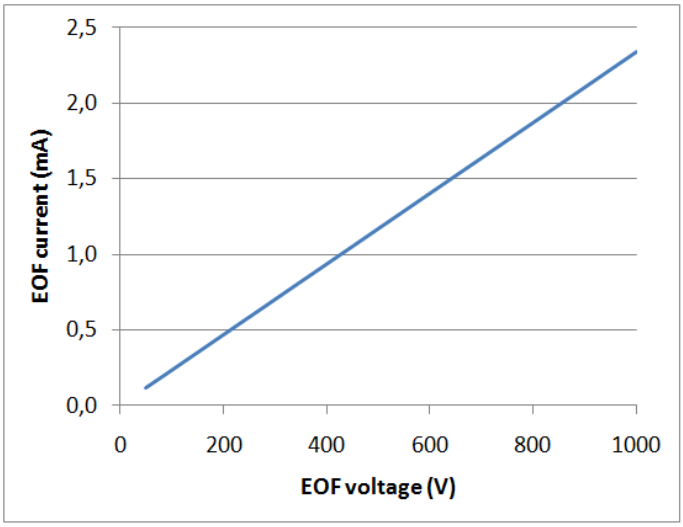

Figure 16: The current through the channels as a result of the applied EOF driving voltage. The dependency of the current on the trap constriction length is insignificant and therefore this model can be used for the 4 types of the chip available.

To calculate the current through the EOF network, the main channel crossing is left out of the equation. The large dimensions will provide a resistance that does not contribute significantly to the total resistance of the side networks. Also, the variation of the trap length has a neglectible influence on the current, because the resistance of the channels is dominant. The total current varies with 0.3% between the use of 0 μm and 30 μm constrictions. Table 10 lists the structures

Table 10: Electrical resistance of the traps and analysis network. The flow rate and current are given for a driving voltage of 100 V. The trap is modeled as a rectangular structure with a length × width of 4 μm × 4 μm.

Channel structure	Structure length (μm)	Resistance (kΩ)	Electric field (V/cm)	Flow rate (mm/s)	Current (mA)
Analysis channel	7585	471	63.5	0.47	0.2
Constriction + transition	4	3.1	800	5.9	0.2
	8	6.2	797	5.9	0.2
	14	10.9	793	5.9	0.2
	34	26.4	781	5.8	0.2

with their flow rate, current, electric field and electric resistance.

The EOF flow rate provides the movement of the liquid in the microchannels, but the movement of specific analytes in this buffer also depends on their electrophoretic velocity:

$$v_{ep} = \mu_{ep} E \tag{16}$$

with μ_{ep} the electrophoretic mobility:

$$\mu_{ep} = \frac{z}{6\pi\eta r} \tag{17}$$

in which z is the charge of the analyte and r is its Stokes radius:

$$r = \frac{k_B T}{6\pi\eta D} \tag{18}$$

where k_B is the Boltzmann constant, T the temperature and D the diffusion coefficient.

The combined velocities of electroosmosis and electrophoresis provides the flow velocity of the analyte in the channel:

$$v_{analyte} = v_{eof} + v_{ep} = (\mu_{eof} + \mu_{ep}) \cdot E \tag{19}$$

The movement of the analytes depend strongly on their charge, for example biomolecules such as DNA and RNA as well as the calcein that is used in this work, are negatively charged. This causes the electrophoretic and electroosmotic forces to act in the opposite direction and the EOF has to exceed the electrophoresis in order to move the analytes in the analysis channels. Therefore, the EOF should be established reliably, with constant buffer conditions and in a material with a well-defined surface charge, ensuring that the electroosmosis is dominant and predictable. Furthermore, for a well-defined EOF to be established, the hydrodynamic flow should be fully suppressed.

4 Results

In this chapter, the results of the experimental work that is done on the microsystem for parallel single cell analysis are presented. First, the fabricated microfluidic ships are shown, which is followed by a description of the sample handling principles on these chips. Next, the results are presented of the protocol implemtentation for cell trapping, cell permeabilization and cell sampling.

4.1 Microfluidic chips

The PDMS chips are fabricated using soft lithography, as mentioned in section 2 of this report. An example of the resulting microchip is shown in figure 17. The chip is filled with ink for the visualization of the structures. From the left, the first photo shows the entire chip as bonded on a glass slide, the second photo gives an overview of the channel networks and the third photo (40× magnification) shows a trap with a 4 μm constriction. The four realizations of the traps are shown in figure 18.

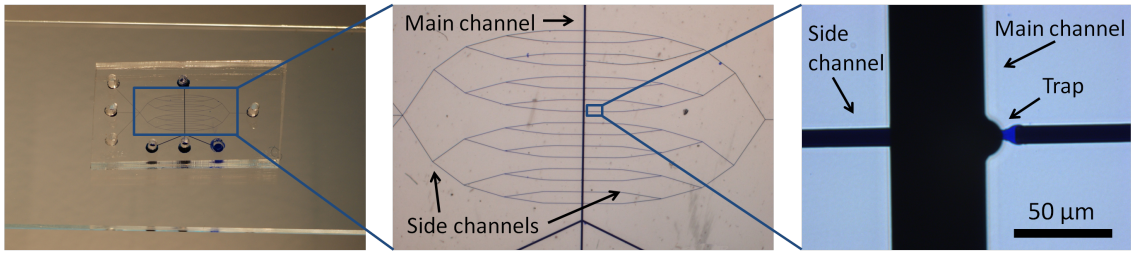

Figure 17: Overview of the PDMS fabricated microsystem. From left to right: the PDMS chip bonded on a glass slide and filled with ink for visualization purposes, an overview of the main channel and side networks, and a 40× magnified photo of a trap having a 4 μm constriction.

The trap constriction layer of the SU-8 is varied in height on two molds, both 2 μm and 3 μm are available.

4.2 Flow control in the microchip

In this section, the three microfluidic flow control approaches are described as used in the different steps of the parallel SCA protocol.

4.2.1 Passive pumping

Cells are introduced into the main channel using passive pumping. This flow is established by providing the inlet and the outlet with droplets (the inlet and outlet numbers can be found in figure 7). Inlet 4 is provided with 15 μL of HEPES buffer and inlet 3 with 1.5 μL of a cell suspension. The cells move through the inlet by gravitation, after which they enter the channel with the established flow. Subsequently, they flow at 100 - 200 μm/s through the main channel and this rate declines with time because the cell suspension droplet depletes. After 1 min of flow, the flow rate is measured as illustrated in figure 19. The time interval between two pictures is 2.4 s and the distance between two traps amounts 300 μm. This corresponds to a flow rate of approximately 125 μm/s.

The manipulation of the flow with passive pumping is demonstrated further by using the four main channel inlets for establishing a flow of fluorescein that is focused in the vicinity of the traps. Inlets 1, 2 and 4 are provided with respectively 4, 4.5 and 20 μL of HEPES buffer and inlet 3 with 1 μL of 1 mM fluorescein in 10 mM HEPES. Since structure length A is longer than structure length B, it is expected that inlet 1 needs a smaller droplet than inlet 2 to offset the higher resistance of

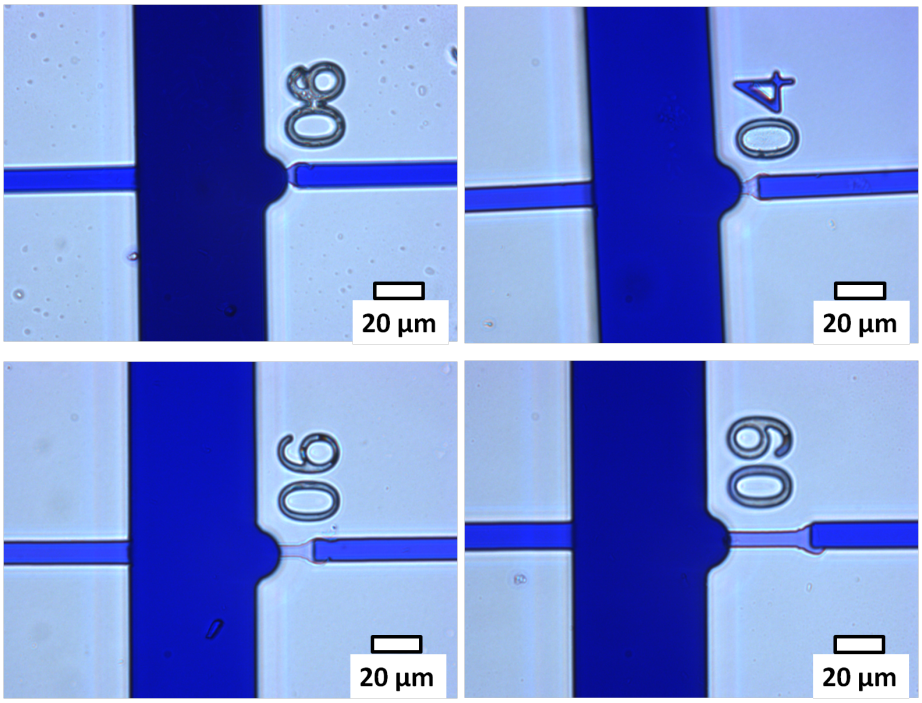

Figure 18: Microscope images (40× magnification) of the trapping structures with a varying constriction length. From top-left to bottom-right, this length is 0 μm, 4 μm, 10 μm and 30 μm.

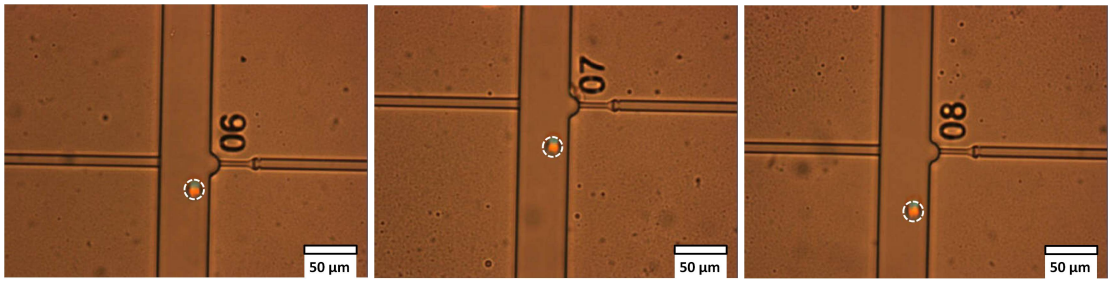

Figure 19: Determination of the flow rate established with passive pumping when the chip is loaded with 1.5 μL of cell suspension on inlet 3 and 15 μL of HEPES buffer on inlet 4. The distance between 2 traps is 300 μm and the time between 2 pictures is 2.4 s, resulting in a flow rate of approximately 125 μm/s.

the former. The exact volumes of these droplets are subsequently determined by experimentation. The flow pattern that arises is shown in figure 20A. This pattern seems to provide an added value over the first approach of using only two inlets. The flow is split and the content from inlet 3, which will later contain the cells, is focused in the direction of the traps. However, this focusing effect is established only at the beginning of the main channel, and when it proceeds the content of inlets 1 and 3 are mixed. Furthermore, the flow pattern is stable for a short period of time. After 2 min, this focusing effect disappears and the fluorescein will move towards both inlets 1 and 4 because the droplet on inlet 1 depletes (see figure 20B).

Therefore, the first approach of using two inlets for the establisment of the flow is the most attractive approach. This involves closing inlets 1 and 2 and using a single inlet and outlet configuration for establishing a controlled flow at a low flow rate.

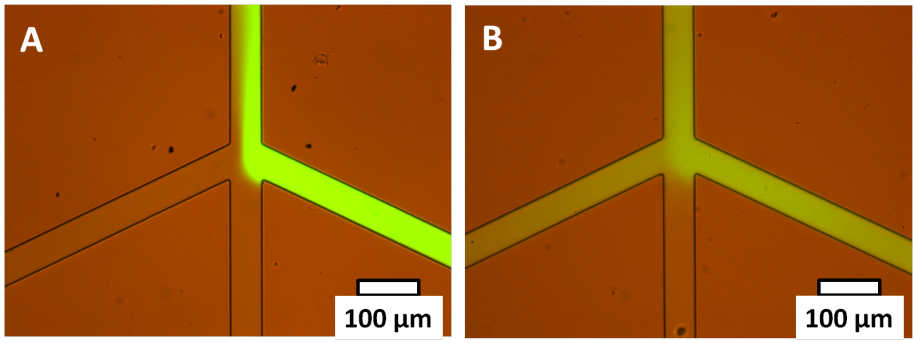

Figure 20: Focusing fluorescein towards the traps using passive pumping. A: Flow pattern that arises shortly after loading the inlets. Inlets 1, 2 and 4 contain respectively 4, 4.5 and 20 μL of HEPES buffer and inlet 3 contains 1 μL of a 1 mM fluorescein solution. B: situation after 2 min. The focusing effect disappears and the flow moves towards both inlets 1 and 4, because the droplet on inlet 1 depletes.

4.2.2 Pressure driven flow

The introduction of the permeabilization solution and the HEPES buffer is performed with a pressure driven flow (PDF) using a syringe pump. Figure 21 indicates the structures and inlets of the main channel, and the direction of the flow. The syringe pump is connected to inlet 2 and now the main channel contains two inlets left open (3 and 4). A 5 μL droplet of the target solution is placed on inlet 4 and introduced in the channel by suction with the syringe pump. For immobilized cells being kept in place with -10 mbar pressure, the flow rate through the main channel structure C has to be limited to around 1 μL/min. The ratio of the fluidic resistance of the structures C/A = 1.7, meaning that the flow rate through the two structures also scales with this factor (both the fluidic resistance and the flow rate scale linearly with the structure length and the other dimensions are equal). A flow rate of 2 μL/min is set with the syringe pump, so the flow rate through structure C equals 2/2.7 = 0.74 μL/min and the flow rate through structure A is 1.26 μL/min.

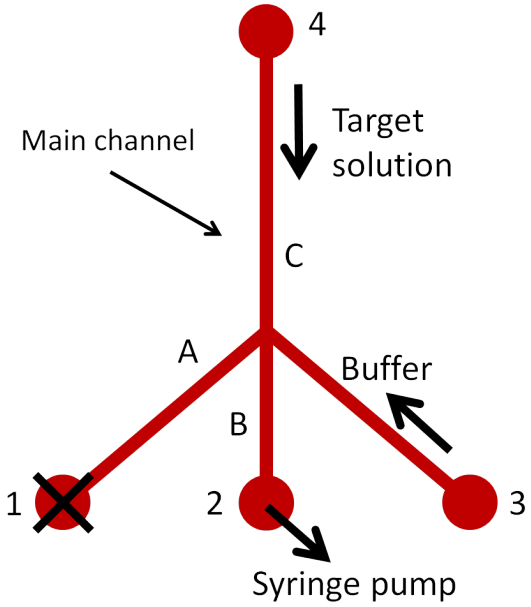

Figure 21: Schematic picture showing the main channel with the indications for the structures and inlets. The syringe pump is connected to inlet 2 (suction) and the buffer and permeabilization solutions are introduced with droplets on inlets 3 and 4, respectively. Inlet 1 is closed.

Figure 22 shows a time-lapse measurement of the introduction of fluorescein using a PDF with the syringe pump using the inlets as shown in figure 21. The measurement starts when the syringe pump is switched on (0 s) at a flow rate of 2 μL/min. The fluorescence intensity starts to increase after 5 s, and after 1 min no change in the fluorescence intensity in the main channel is observed anymore. This suggests that the flow at 2 μL/min has to be maintained for 1 min in order to achieve a solution exchange in the main channel.

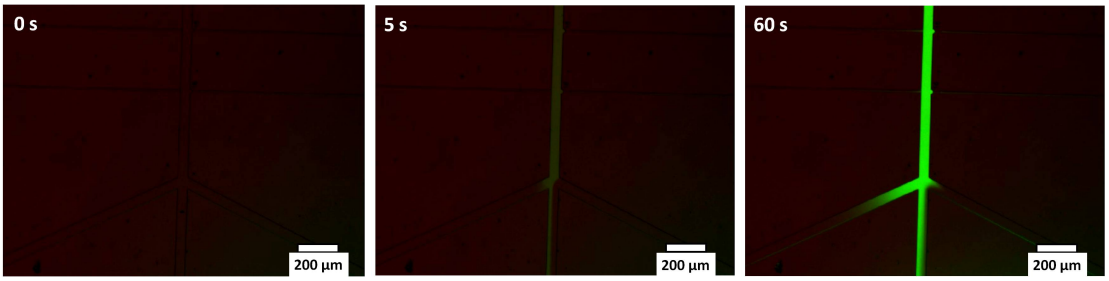

Figure 22: Filling of the main channel with a 1 mM fluorescein solution using a PDF. Fluorescein is introduced from inlet 4 and HEPES buffer is introduced from inlet 3. The syringe pump is connected to inlet 2, employing suction at a flow rate of 2 μL/min. From left to right: time-lapse images starting at 0 s.

4.2.3 Electroosmotic flow

The EOF that is applied for cell content transportation is modeled in chapter 3. Two methods are employed for characterizing the established flow. First, the flow is visualized using a 1 mM fluorescein solution. Second, the current that results from the EOF driving voltage is measured.

For the optical verification, 5 μL of fluorescein solution is introduced from inlet 6 and also 5 μL of HEPES buffer is placed on inlet 8 to suppress the hydrodynamic flow. The driving voltage is set to 800 V between inlets 6 and 8. This voltage is chosen for the purpose of achieving a high enough flow rate for visualization of the EOF establishment. Since the inlet is initially filled with approximately 0.8 μL of buffer, the loading of a new solution using EOF is time-consuming. Therefore, in the cell analysis experiments, EOF is only used for transportation of species already present in the channels.

Figure 23 shows the inlets as used for the EOF establishment. The entry of fluorescein is shown in figure 24 at the locations indicated in figure 23.

A time-lapse measurement using five points in time is employed to determine the flow rate in a straight structure of the analysis channel (structure 'c' in figure 7), as shown in figure 25. In every picture, the location of the highest fluorescence intensity is determined using the image analysis software package ImageJ (rsb.info.nih.gov/ij). The time interval between every picture is known and therefore the flow rate can be determined. This results in an average rate of 91 μm/s, with lower values of 70μm/s near the corners and a high value of 120 μm/s in the middle. The corners in the side network slow down the flow due to the fringing effects of the electric field, resulting in a varying flow rate through the side networks.

According the the model described in chaper 3, the flow rate when a 800 V driving voltage is applied is expected to be around 3.8 mm/s (figure 15). This means a discrepancy with a factor 40 between the calculation and the measurement. It was already anticipated for that the EOF as a flow control mechanism is poorly compatible with the PDMS material. The flow rate is not stable as a function of the applied voltage, causing large variations in the flow rate over time. This is likely due to the inhomogeneous surface charge of PDMS, which can change in time and which is also affected by the BSA coating [31].

A small variability in the flow rate is not a problem when the EOF is applied for the transportation of cell content. A high level of control is required over the moments in time the flow is switched and this can still be achieved in the current situation. This preliminary experiment

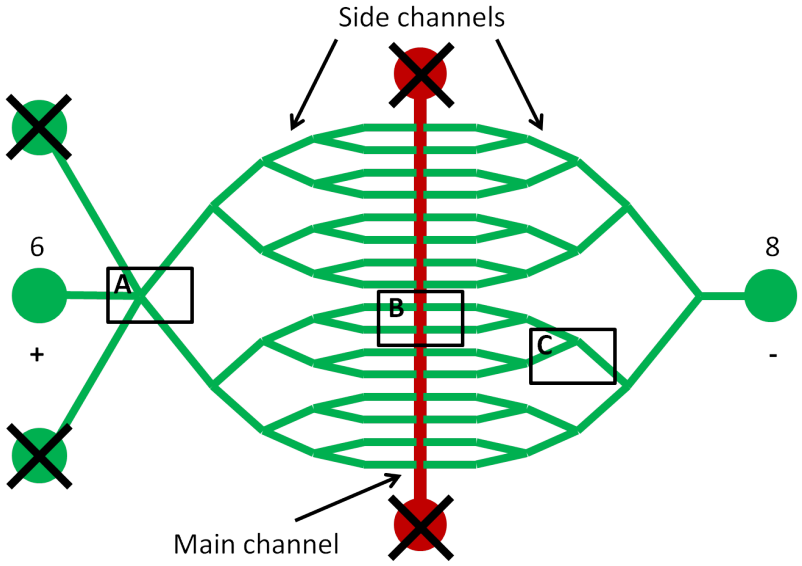

Figure 23: Schematic picture showing the inlets as used for the EOF establishment. An 800 V driving voltage is applied between inlets 6 and 8. The main channel inlets as well as inlets 5 and 7 are closed to suppress the hydrodynamic flow. The locations at which the pictures from figure 24 are taken are indicated with the black rectangles.

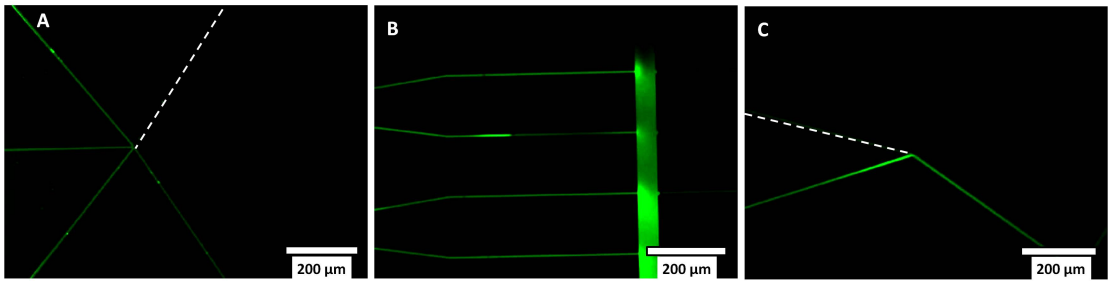

Figure 24: Visualization of the EOF through the side networks using 1 mM fluorescein (introduced from inlet 6). The driving voltage (800 V) is applied between inlet 6 and inlet 8. A: area near inlet 6. B: injection of fluorescein into the main channel. C: area near inlet 8.

shows that it is possible to establish an EOF in the analysis channels of the chip when filled with HEPES buffer. When this concept is applied for parallel SCA, a permeabilized cell will be located in the trap, changing the electric field distribution in the analysis network. How this will affect the flow is not clear and this must be investigated in the future.

The second method of EOF characterization involves current measurements. For driving voltages of 50, 100, 200, 500 and 100 V, the current through the channels is measured and plotted in figure 26. The relation between the measured current and the applied voltage is approximately linear. However, the measured current is on average 40 times lower than the current predicted by the model (see figure 16). Combining this with the factor 40 discrepancy in the calculated and measured flowrate, it is assumed that a structural mismatch between the model and the measurement data exists. Since the current only depends on the electrical resistance of the channel, this suggests the existence of some clogging or local channel collapse. The EOF characterization can proceed when materials are used that allow a more accurate control over the EOF conditions.

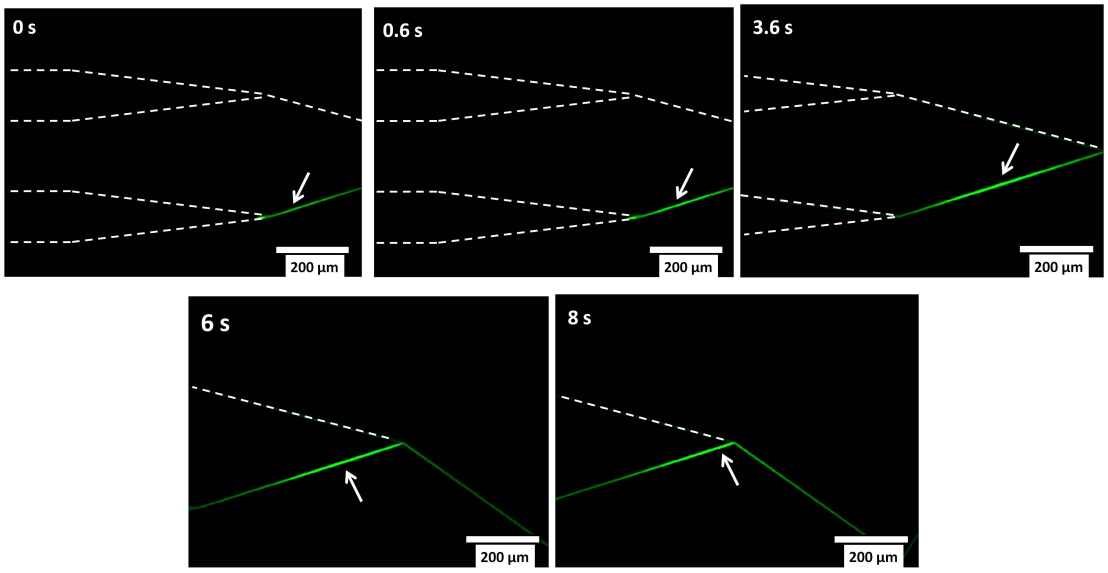

Figure 25: Measurement of the EOF flow rate in the analysis network when a 800 V driving voltage is applied between inlets 6 and 8 (structure 'c' in figure 7). The speed varies between 70 μm/s and 120 μm/s, with an average of 90 μm/s.

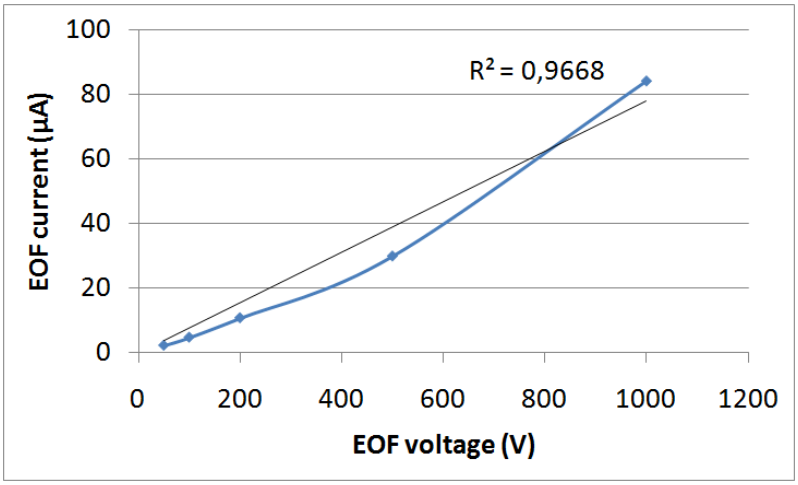

Figure 26: Current measurement as a function of various EOF voltages. The behaviour is with a good approximation linear, as expected, but the value of the current is on average 40 times lower than predicted by the model (see figure 16).

4.3 Cell trapping

The first step of the protocol for parallel single cell analysis is single cell trapping. The cells are introduced in the chip with a concentration of $\sim 10^7$ cells/ml in 10 mM HEPES using passive pumping. Once loaded, they are trapped in dedicated structures with the help of an externally applied pressure. The trap consists of a circular shaped pocket (20 μm diameter) in which the aperture of the trap constriction is located. This constricion is 4 μm wide and both its length and its height are varied. Four constriction lengths are incorporated in the mask design (0, 4, 10 and 30 μm) and two constriction heights are available (2 and 3 μm) as a result of the fabrication process, giving eight different types of chips. These two design parameters are expected to have an important effect on the trapping efficiency. The cells are trapped using a negative pressure applied by the Maesflo pressure controller. This pressure is optimized during the trapping experiments

and varied in a range of -20 to -50 mbar, causing some discrepancy in the trapping efficiency data. The optimal pressure is determined to be -30 mbar and this is used for most of the experiments. The influence of these parameters on the trapping efficiency is studied by testing multiple chips ($\geq$3) of every type.

The trapping efficiency is defined as:

$$Efficiency = \frac{\#_{traps,filled}}{\#_{traps,total} - \#_{traps,clogged}} \tag{20}$$

When a trap is not operational due to clogging, it is left out for the efficiency calculation by subtracting it from the total amount of traps available. Clogging can occur due to PDMS particles released in the main channel after punching the reservoirs. Also, an analysis channel can be clogged due to particles that end up in the structures during the plasma bonding. Although these traps are removed from the efficiency calculations, they still decrease potential throughput when parallel analysis is to be done on a larger scale. Therefore, a different chip material has to be used. When molding the chips from polystyrene (PS) for example, no reservoirs are to be punched and by preparing the chip in a clean environment, the amount of clogging can be drastically reduced. Furthermore, PS is biocompatible, cheap and rigid, allowing better defined structure sizes. PDMS is used here because it is a good material for prototyping; its fabrication is easy, fast and cheap.

The trapping efficiencies for the eight types of chip are shown in figure 27. For every type of chip, the efficiency is shown for single cell trapping, multiple cell trapping and the combination of both. The highest total trapping efficiency is achieved with a 0 μm constriction length, regardless the constriction height. When comparing the "shallow" traps (2 μm) and the "deep" traps (3 μm) on the total performance, there seems to be no significant difference and the precise trapping behaviour depends on the constriction length. For the 3 μm high traps, the efficiency depends little on the constriction length and is on average 90%. The shallow traps perform best in combination with a 0 μm constriction, also achieving a 90% efficiency.

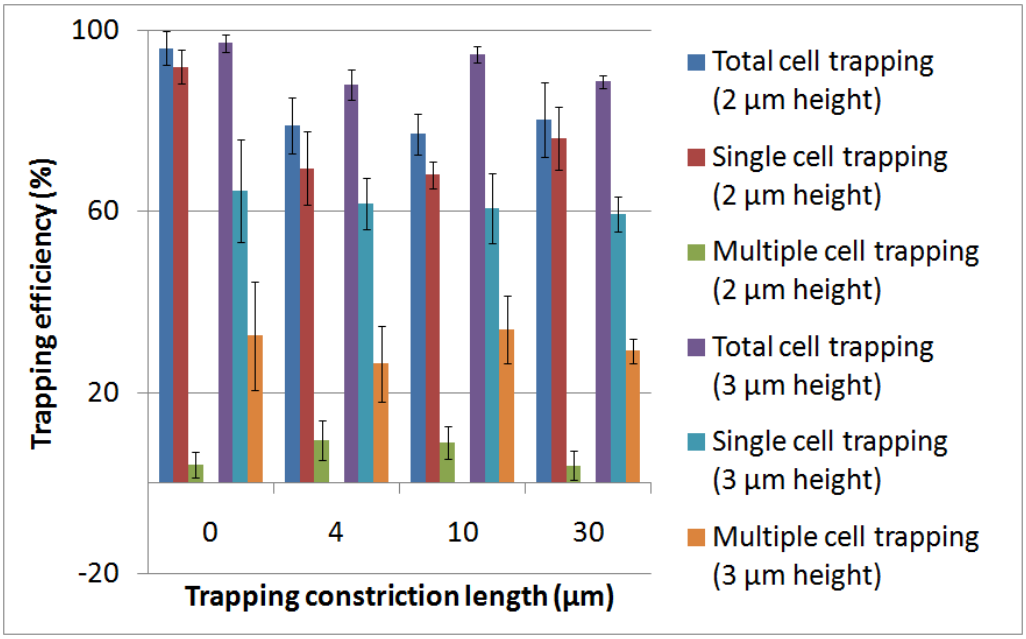

Figure 27: Trapping efficiency of eight types of chip, having traps with different constriction heights (2 and 3 μm) and lengths (0, 4, 10 and 30 μm). For every type, the total trapping efficiency, the single cell trapping efficiency and the multiple cell trapping efficiency is shown. At least three chips are used for every type.

For the purpose of parallel SCA, it is interesting to study the efficiency of single cell trapping compared to the trapping of multiple cells. Multiple cells are trapped if the constriction aperture

is not sealed completely by the cell that enters the trap first. It can also occur if the first trapped cell is too small to fill the pocket, leaving room for a next cell to be captured in the trap. Single cell trapping efficiency is in general higher when shallow traps are employed (figure 27). The 0 μm and 30 μm constriction lengths show the highest single cell trapping efficiency and for the deep traps this seems to be independent of the constriction length. The multiple cell trapping efficiency is in general high with deep traps, also independent of the constriction length.

Besides multiple cell trapping, another interesting behaviour is the "trapping loss". This occurs when a trapped cell squeezes itself through the constriction of the trap into the analysis channel. This behaviour is shown in figure 28. Losses are the highest with shallow traps in combination with the 0 μm constriction. For the remaining three constriction lengths, the deep traps show higher losses.

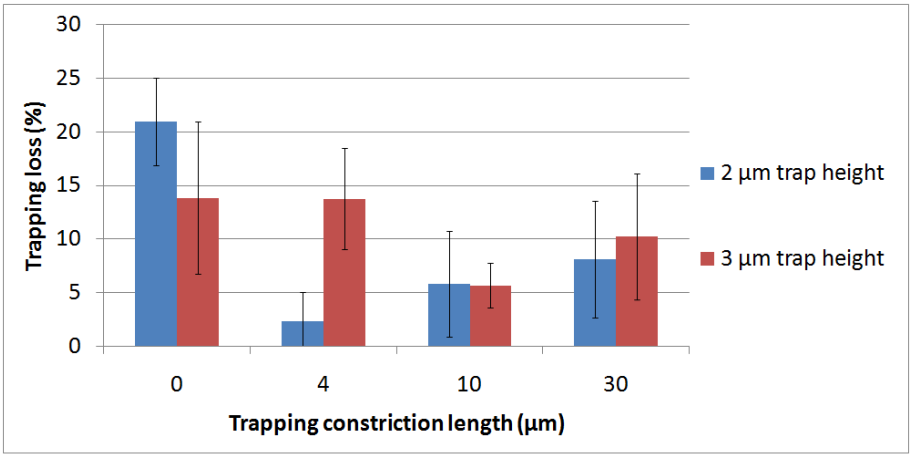

Figure 28: Trapping loss (movement of cells through the traps and into the analysis channel) of chips using traps with different constriction heights (2 and 3 μm) and lengths (0, 4, 10 and 30 μm).

The performance of the chips is obtained when the trapping loss is subtracted from the single cell trapping efficiency, as shown in figure 29. The performance is in general higher for the shallow traps, 60-70% trapping efficiency compared to 50% for the deep traps. The constriction length does not have a significant influence on the trapping performance.

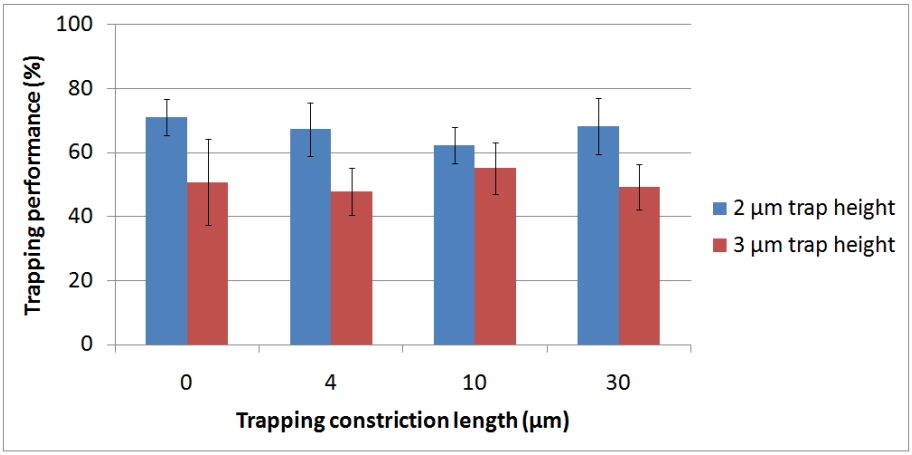

Figure 29: Trapping performance (single cell trapping efficiency - trapping loss) of microchips using traps with different constriction heights (2 and 3 μm) and lengths (0, 4, 10 and 30 μm).

In conclusion, the shallow traps perform better than the deep traps and the highest single cell trapping efficiency is obtained with a 0 μm trap constriction (90%). However, the trapping loss

is also the highest for this type of trap. Still, depending on the precise application of the parallel SCA platform, this trapping loss may not be a problem as long as the cells moved in the analysis channels are removed before the permeabilization step.

Cell trapping can occur in two basic modes, as discussed in figure 8. Either the cell is retained in front of the trapping aperture or it is squeezed in the trap constriction. These two modes are shown in figure 30. For all of the four constriction lengths, the trapping mode has important consequences during the next steps of the cell analysis protocol. In trapping mode 2, the cell is secured more tightly in the trap, reducing the risk of being flushed away. However, the extent to which the cell is squeezed in the constriction also determines the amount of accessible membrane surface area, influencing directly the membrane permeabilization. Unfortunately, the way in which the cell sits in the trap can not be controlled, which introduces a random factor in the cell analysis protocol.

This protocol has shown to provide easy and reproducible cell trapping. The concept is easily scalable due to the chosen arrangement of the traps in the microfluidic chip. Fast parallel cell trapping is achieved within 2-5 min while providing reliable control over the flow and the pressure applied.

4.4 Membrane permeabilization

The second step for parallel SCA is the permeabilization of the cell membrane, which is done using the three approaches subsequently discussed. Two types of chemical approaches are tested. First, 10 μg/ml digitonin is used for reversible permeabilization and second, 1% LiDS is employed for irreversible cell lysis. Alternatively, electrical lysis is demonstrated during the optimization of the EOF driving voltage.

After the cells have been trapped, the permeabilization solution is introduced using the syringe pump at a flow rate of 2 μL/min for circa 1 min. During this solution exchange, the trapping pressure of the Maesflo system is reduced from -30 mbar to -10 mbar to relieve the stress from the cells, while avoiding them to be flushed out of the traps. After the solution is loaded, the trapping pressure is switched off.

The first permeabilization solution is 10 μg/ml digitonin in a Ca^{2+}-free solution, providing reversible permeabilization. First, the digitonin permeabilization time (t_p) has to be determined experimentally for optimal exposure of the cell to the digitonin solution. This is done by time-lapse imaging of the cells and the visualization of PI entry or calcein release. Figure 31 shows selected snapshots of this process. t=0 is defined as the moment the flow is switched off after introduction of the permeabilization solution. The first 3 min, the cell is swelling progressively and after 3 min the PI entry becomes visible. The cell swelling indicates that small pores are created first, and only after 3 min they are big enough to allow the PI to enter the cell. Furthermore, enough PI molecules need to enter for visualization. The permeabilization time is measured for 20 cells, yielding an average value of 3.5 min.

The fluorescence intensity from figure 31 as a function of the time is plotted in figure 32, after subtraction of the background fluorescence. The measurements are carried out in ImageJ. Also, the surface area increase of the top view of the cell is shown, representing the cell swelling rate (increase of the surface area with respect to t=0). Cell swelling and permeabilization processes occur in tandem with each other.

The permeabilization process is affected by the cell trapping mode. The digitonin can access the portion of the membrane that faces the main channel and the trapping pocket. In trapping mode 1, the cell is sitting in front of the trap and therefore the entire cell membrane is accessible. In trapping mode 2, the cell is partly squeezed in the constriction and subsequently, the membrane is permeabilized only partially. Therefore, homogeneous permeabilization is achieved only in trapping mode 1. This difference in permeabilization efficiency is illustrated in figure 33 with

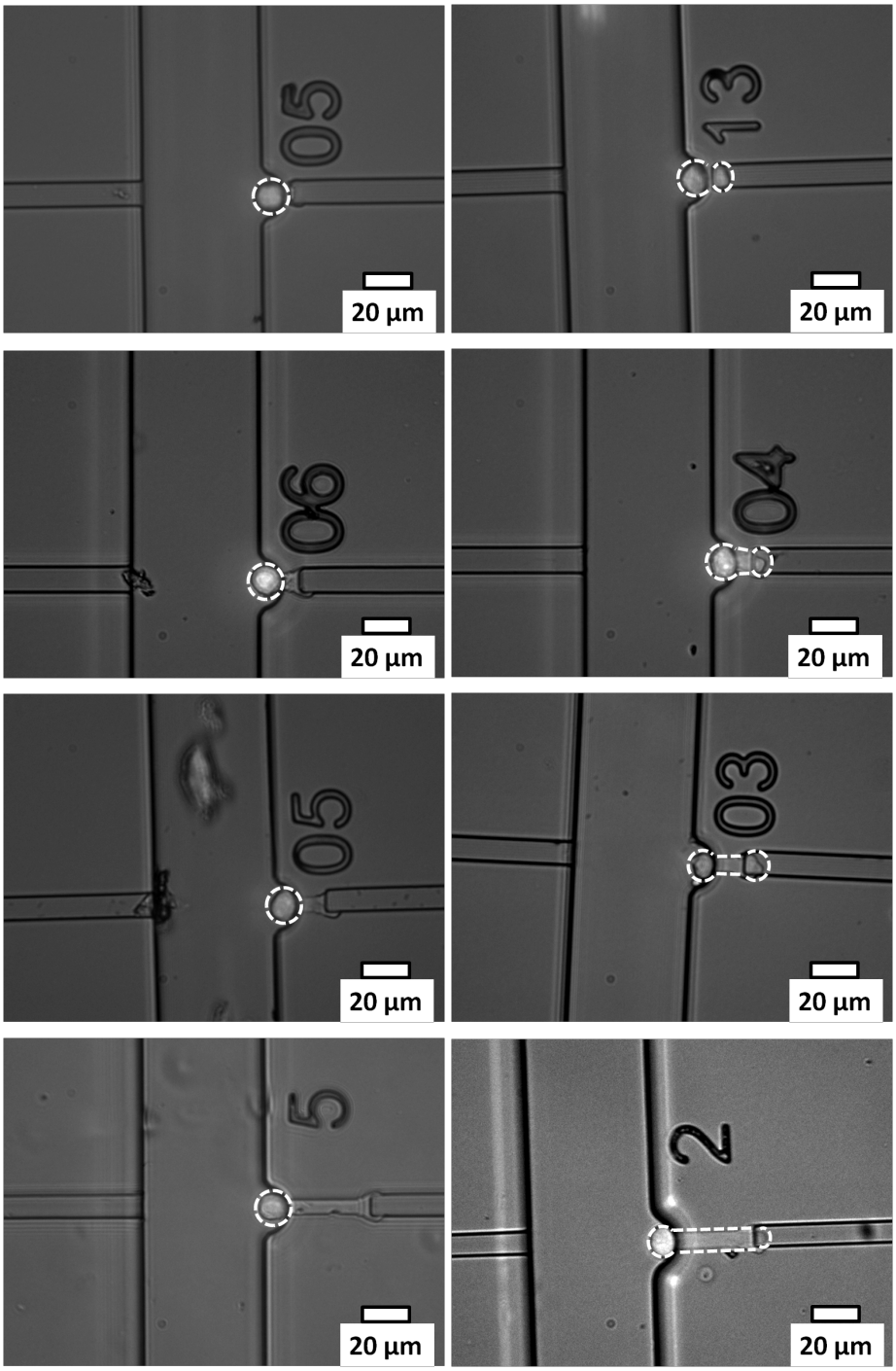

Figure 30: Two different trapping modes are observed. Here, chips contain a 3 μm constriction height. Left: cells are immobilized in front of the traps. Right: cells are squeezed in the trap constriction. From top to bottom: the various trap constriction lengths (0, 4, 10 and 30 μm).

the PI entry in calcein stained cells. In figure 33A, a cell is trapped in mode 1 and the digitonin has permeabilized the membrane homogeneously (t_p=3.5 min). The cell is coloured yellow, indicating the entry of PI in the cell over its full membrane surface area and the release of calcein in both the main and the analysis channels. In figure 33B, the cell is trapped in mode 2 and the digitonin only accesses a portion of the membrane (t_p=4 min). The portion of the cell sitting in front of the trap is yellow, indicating a locally permeabilized membrane that allows PI entry. In the green part of

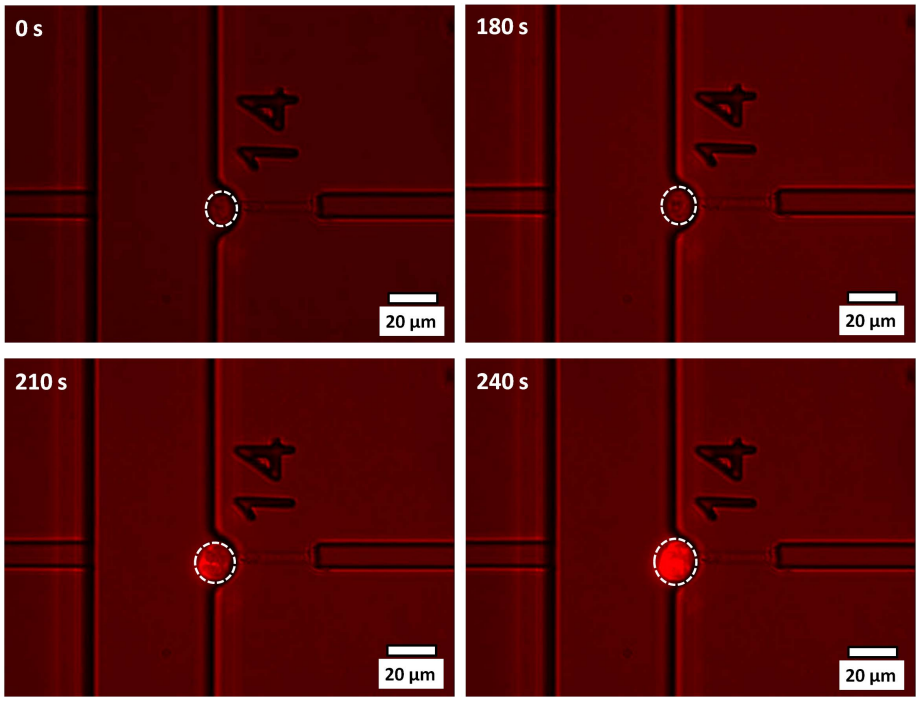

Figure 31: Permeabilization of trapped cells with 10 μg/ml digitonin in HEPES, supplemented with 10 μg/ml PI. At t=0 s, the flow introducing digitonin in the main channel is switched off after 1 min pumping at 2 μL/min. The first 3 min of the measurement, the cell is swelling progressively. After 3 min, the PI entry starts and after circa 3.5 min the cell is fully permeabilized.

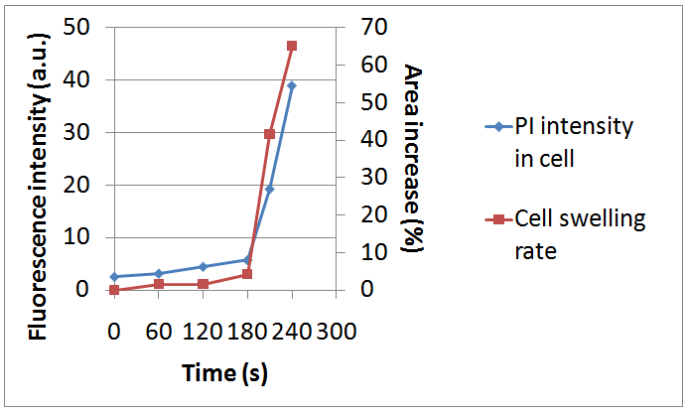

Figure 32: Digitonin permeabilization process is measured with the fluorescence intensity of PI (using ImageJ). Also, the cell swelling is included, which occurs in tandem with the PI entry.

the cell, the membrane is left intact and no calcein release or PI entry takes place. Using ImageJ, the calcein release in the analysis channels from figure 33A is determined to be 57% more intense compared to figure 33B. The areas of measurement are indicated. Figures 33C and D show a cell trapped in mode 2 and squeezed in the trap constriction. The digitonin has permeabilized the membrane in the main channel (t_p=2 min), allowing the entry of PI. Figure 33C is taken shortly after t_p and initially, a similar phenomenon as in figure 33B is observed. The permeabilized part of the membrane is yellow and the part in the constriction is green, indicating permeabilization of the part facing the main channel. Figure 33D shows the slow diffusion of PI through the cell, reaching the part that is squeezed through the trap constriction after approximately 2 min. In figures C and D, no calcein is released in the side channel and the calcein in the cell is thought to

have photobleached.

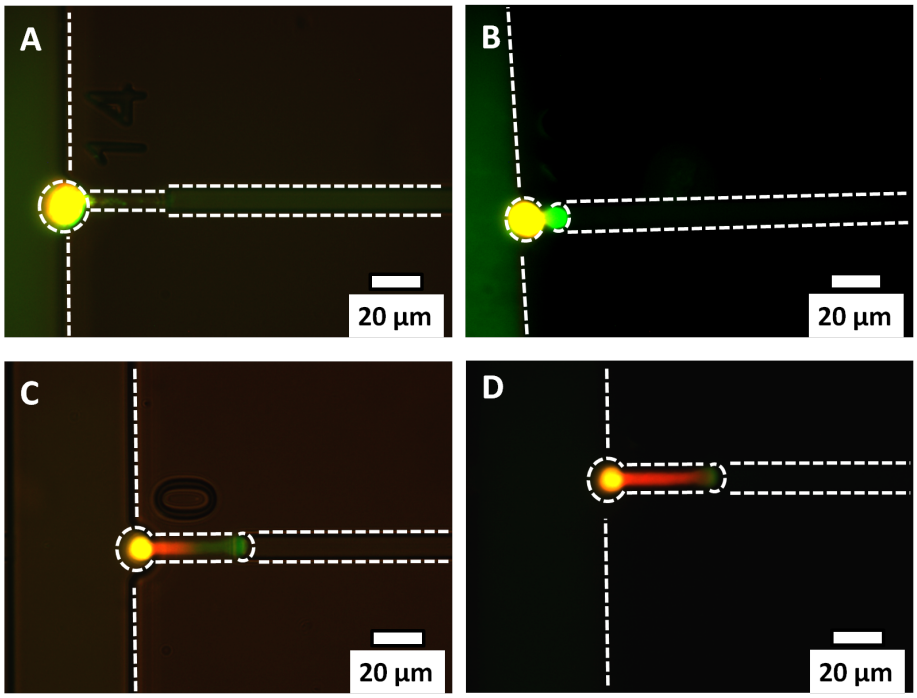

Figure 33: Digitonin-based permeabilization of a trapped cell: influence of the trapping mode. Cells trapped in 2 μm high structures are exposed to digitonin and show permeabilization shortly after PI entry. A: trapping mode 1 in a 0 μm constriction, leading to homogeneous permeabilization (t_p=3.5 min) and showing calcein release. B: trapping mode 2 in a 0 μm constriction, leading to partial permeabilization (t_p=4 min) and showing 57% less calcein release in the analysis channel compared to A. C and D: trapping mode 2 in a 30 μm constriction with a time interval of 2 min. After permeabilization (t_p=2 min), PI diffuses to the portion of the cell that is squeezed in the trap constriction.

The second chemical permeabilization approach consists of lysing the cells using 1% LiDS in PBS. Cell lysis takes place in the first 10 - 20 seconds after its introduction of the detergent, making it a fast and reproducible method for destructive permeabilization.

Figure 34 shows snapshots from the cell lysis process. The lysis time is determined from the release of calcein out of the cell and time measurement starts after LiDS is introduced for 1 min at 2 μL/min. The major fluorescence intensity drop occurs within the first 10 s after exposure to LiDS, followed by a gradual decrease in intensity as the calcein diffuses out of the cell.

Calcein release merely occurs in the main channel, as seen in figures 34 and 35. Since the cell is trapped in mode 2, LiDS destroys the portion of the membrane in the main channel and calcein is released before the detergent diffuses in the trap constriction. Therefore, no fluorescence is observed in the analysis channel. This is verified by measuring the fluorescence intensity in the cell, in the main channel and in the analysis channel using ImageJ (see figure 35). If this approach is applied for cell analysis, all the molecular information contained in the cell will be lost by diffusion in the main channel and therefore this approach of permeabilizing cells trapped in mode 2 cannot be employed for a reliable analysis.

As an alternative approach, cells can also be lysed by applying an electric field. As before, the parameters of cell lysis are determined, and potentials of 50, 100, 200, 500 and 1000 V are applied on the EOF electrodes (inlets 6 and 8) for a certain Δt. Figure 36 shows pictures of a calcein stained cell after application of 100 V for 1 min, 500 V for 1 min and 1000 V for 15 s. The cell is trapped in mode 2, which would prevent homogeneous permeabilization when chemicals are used. However, homogeneous electrical lysis is obtained in 15 s with the application of 1000

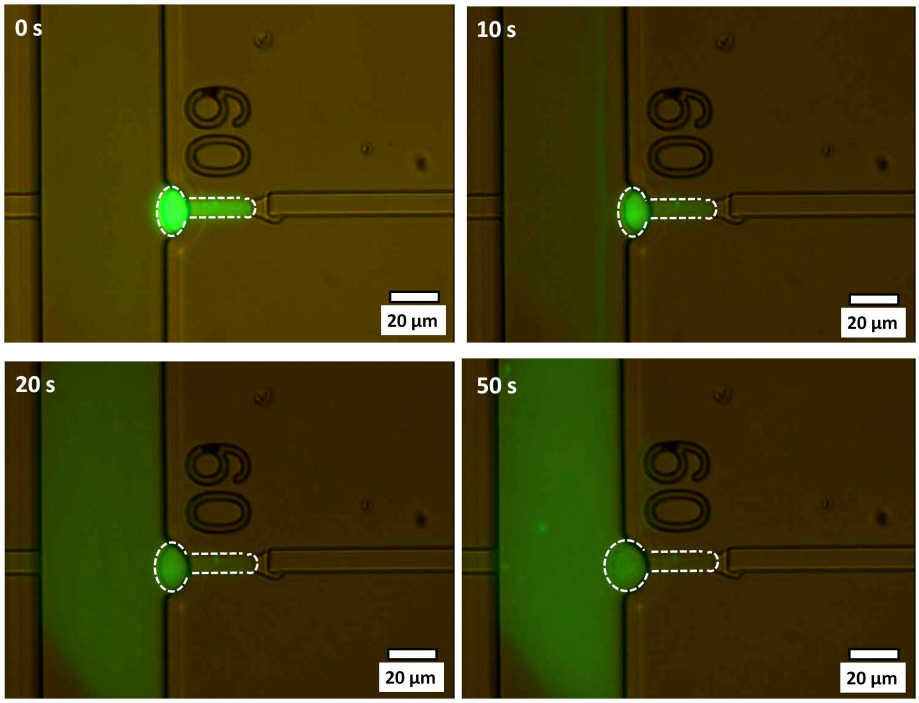

Figure 34: Lysis of a trapped calcein stained cell with 1% LiDS in PBS. Time measurement starts after introducing LiDS (t=0 s). The cell lysis is shown using pictures after 10, 20 and 50 s of exposure to LiDS. Full lysis occurs in the first 20 s of the experiment.

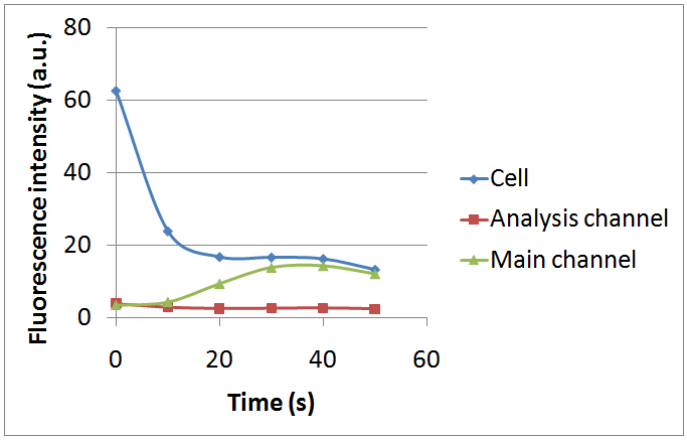

Figure 35: LiDS lysis is monitored by measuring the fluorescence intensity in the cell, the main channel and the analysis channel using ImageJ. The release of calcein takes place in the main channel only.

V on inlets 6 and 8, which is equivalent to 8 kV/cm accross the trap (figure 15).

Although the fluorescence intensity of the cell decreases after application of potentials below 1000 V, it is thought that no poration takes place. The cells are not swelling and no release of calcein in the main channel is observed and therefore these lower voltages do not induce lysis (verified by ImageJ measurements). The fluorescence intensity decrease of the cell is therefore attributed to photobleaching of calcein.

With the chemical approach, the trapping mode has a significant influence on the permeabilization process of the cell. In mode 1, homogeneous permeabilization of the membrane can be achieved and the cell content can be released in the analysis channel. In trapping mode 2, the cell

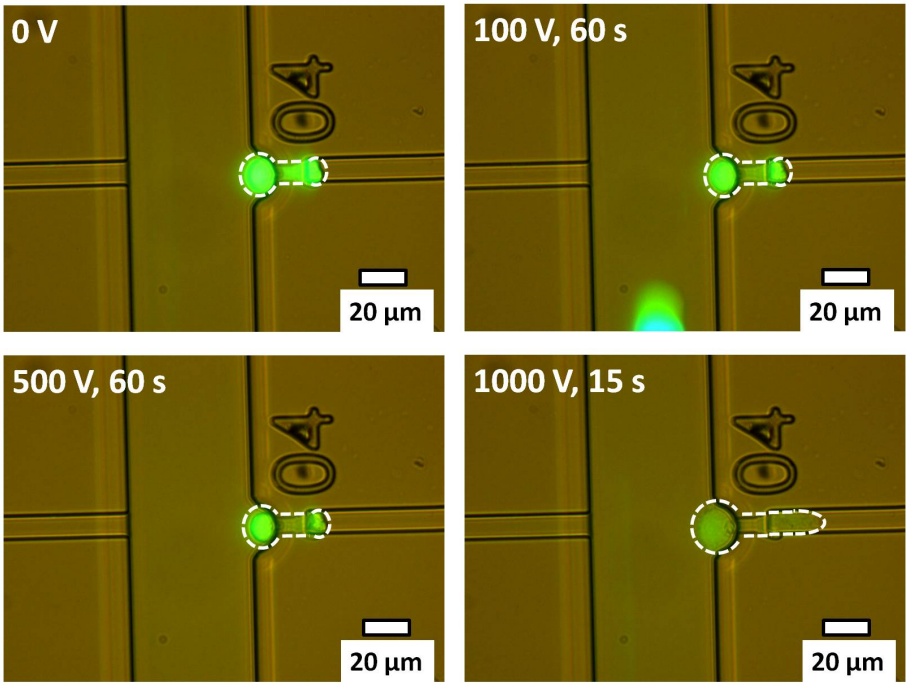

Figure 36: Electrical lysis of a calcein stained cell. From left to right: control (0 V), after 1 min of 100 V, after 1 min of 500 V and, after 15 s of 1000 V.

is secured more tightly in the trap and only the portion of membrane in front of the main channel is permeabilized. Most of the biological information is lost due to diffusion in the main channel. The trapping mode can not be controlled and therefore the succes of the sampling step remains subject to this random event. With electrical lysis, the permeabilization is homogeneous and this is not influenced by the trapping mode.

4.5 Cell sampling

The third step in the cell sampling protocol is the retrieval of the cell content for cell analysis. This is accomplished with the establishment of an EOF in the side channels, dragging the released cellular compounds into the analysis channel. It is expected that the flow rate can not be controlled precisely. The PDMS surface properties are not stable, the hydrodynamic flow can not be fully surpressed and the effect of a cell in the applied electric field is not understood. Therefore, the focus is on a proof-of-principle experiment where calcein is extracted out of the cell and transported in the analysis channel.

A calcein stained cell trapped in mode 2 (see figure 37A) is chemically permeabilized with digitonin, using the average digitonin exposure time t_p (3.5 min) determined in the previous section. Because the digitonin permeabilization is potentially reversible, the EOF electric field should be kept well below the cell membrane breakdown potential. According to the literature, this potential is achieved with an electric field in the low kV/cm range [11], which would be reached by applying 100 V between inlets 6 en 8. Therefore, it is considered safe to use a 50 V driving voltage between inlets 6 and 8 for the EOF, obtaining an electric field of 32 V/cm in the analysis channels.

In figure 38, the calcein transportation from the digitonin-permeabilized cell is shown. Because the cell is trapped in mode 2, the permeabilization is not homogeneous. With chemical permeabilization only, no calcein would be released in the analysis channels as shown in the previous section. However, in combination with the EOF, it is possible to transport the calcein from the digitonin-permeabilized cell in the analysis channel. The time measurement starts as soon as

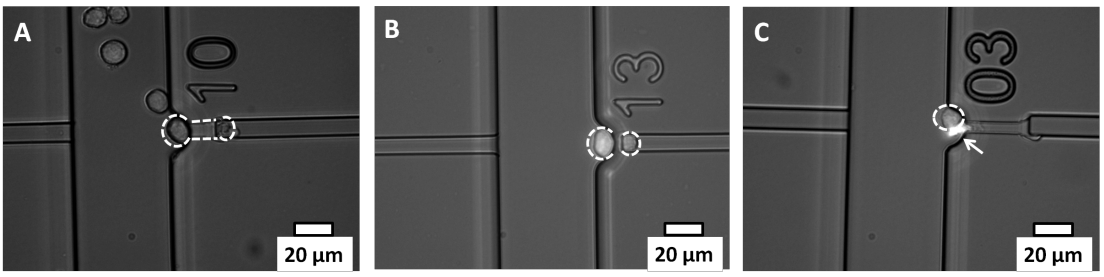

Figure 37: Physical positioning of permeabilized cells in the trap. From left to right: mode 2 trapped cell before digitonin permeabilization (figure 38), mode 2 trapped cell before lysis with LiDS (figure 40) and cell that forms an incomplete seal accross the aperture due to a particle, which is lysed with LiDS in figure 42.

the flow becomes visible and the progressive calcein transportation is shown with intervals of 10 s.

Calcein from the target cell as well as other cells is present in front of the trap, saturating the fluorescence signal in the vicinity of the trapping pocket and the main channel. These parts are therefore left out to emphasize the fluorescence in the analysis channel. Fluorescence intensity is measured using ImageJ to show the progressive release and transportation of calcein in the analysis channel. This measurement is presented in figure 39 for the main channel and the analysis channel. The intensity in the analysis channel shows a sudden increase due to calcein that has already diffused out of the cell. This is followed by a gradual decline, when the initially accumulated amount is transported and the intensity is about to stabilize. In the main channel, the intensity is significantly higher, but there the calcein is released by multiple cells (e.g., cells in the reservoirs or cells sitting in the main channel). In the analysis channel, this intensity is approximately 4 times smaller. It can be seen that not all the calcein from the cell is transported there, meaning that molecular information is lost.

Next, a calcein stained cell trapped in mode 2 (see figure 37B) is chemically lysed using LiDS. The cell membrane is destroyed after exposing it to this detergent for 10 - 20 s. Lysis is irreversible, so possible electrical lysis that occurs when the EOF is established is not a concern. This allows for experimentation with a higher EOF driving voltage to see whether the efficiency of calcein transportation can be increased. The electric field strength in the analysis channels is 317 V/cm. The time measurement starts as soon as the flow becomes visible, and the process is shown using intervals of 10 s.

Figure 40 shows the calcein transportation from the lysed cell. Again, the permeabilization is expected to be non-homogeneous due to the mode 2 trapping. In this trapping mode, it was not possible to obtain calcein in the analysis channels with lysis alone (figure 34). However, the cell content transportation can be achieved with the use of an EOF. In figure 40, the EOF transportation of the calcein is shown with a plot of the fluorescence intensity in the main and analysis channels as a function of time. The fluorescence intensity in the main channel and the analysis channel is measured using ImageJ to visualize the progressive transportation of the sample. The intensity in the main channel is already high before the intensity starts to increase in the analysis channel, therefore showing a delay. This suggests a fast lysis of the cell prior to the establishment of the flow, causing release and diffusion in the main channel before the membrane in front of the trap aperture is lysed. This causes a loss of biological information and also the sample that is to be transported gets contaminated with biomolecules from other cells present in the main channel. After the flow in the side channel is established, the calcein exchange takes place rapidly, clearly depleting the area in front of the trap from calcein.

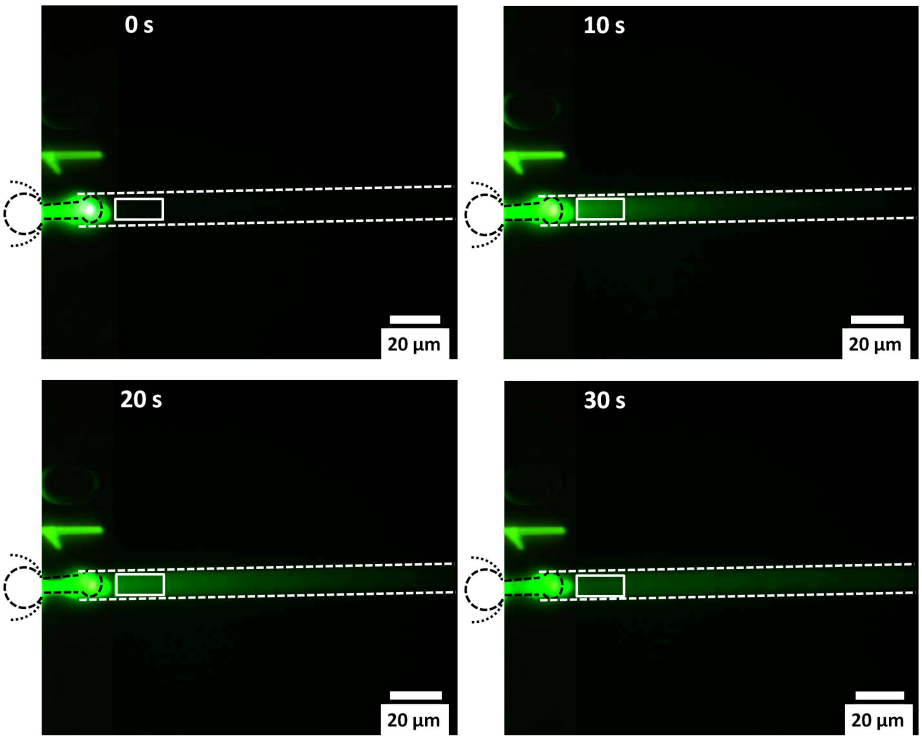

Figure 38: Transportation and diffusion of calcein from a digitonin permeabilized cell that is trapped in mode 2. The EOF is established with a field of 32 V/cm and the time interval between two photos is 10 s. Time measurement starts as soon as the flow becomes visible. The rectangle indicates the area of fluorescence intensity measurement that is used for figure 39.

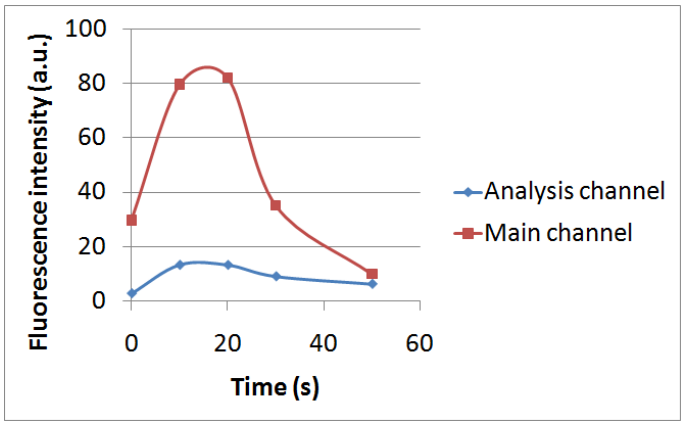

Figure 39: Transportation of calcein after permeabilization with digitonin. The intensity is measured in both the main channel and the analysis channel using ImageJ (see figure 39) and plotted as a function of the time.

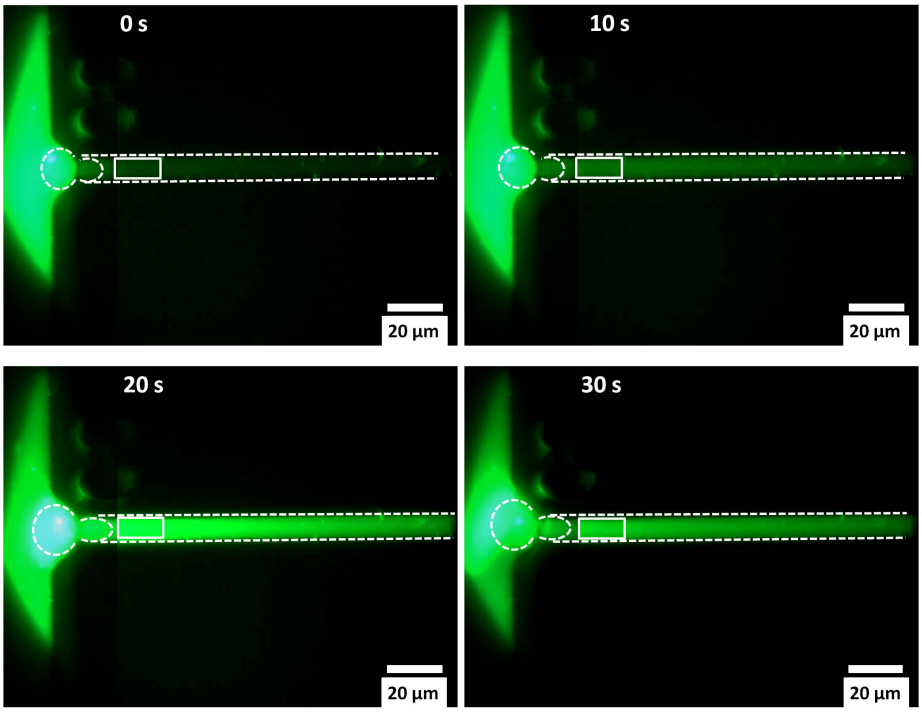

Figure 40: Transportation and diffusion of calcein from a LiDS lysed cell that is trapped in mode 2. The EOF is established using an electric field of 317 V/cm in the side channels and the time interval between two photos is 10 s. Time measurement starts as soon as the flow becomes visible. The rectangle indicates the area of fluorescence intensity measurement that is used for figure 41.

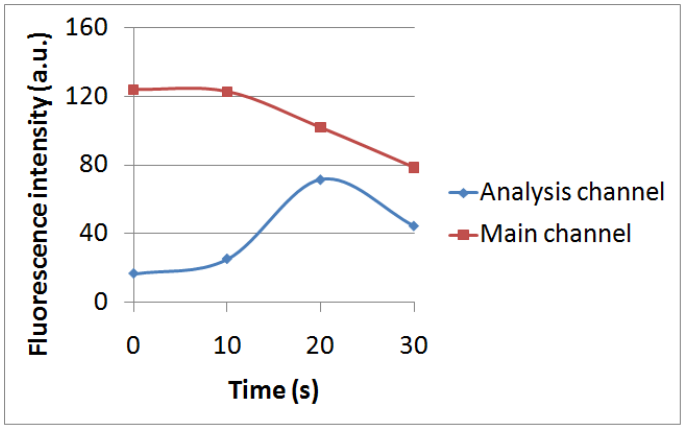

Figure 41: Transportation of calcein after lysis with LiDS. The intensity is measured in both the main channel and the analysis channel using ImageJ (see figure 41) and plotted as a function of the time.

With these experiments, it is shown that although a cell is trapped in mode 2, being squeezed in the trap constriction, still the cellular content can be directed into the analysis channel using a combination of chemical permeabilization and an EOF. However, the amount of fluorescence intensity in the main channel exceeds in both cases the intensity in the analysis channels. This can be due to the different structure sizes, since the main channel is 5 times higher than the analysis channel. Therefore, the amount of calcein in the main channel is much larger, resulting in a higher fluorescence intensity.

Digitonin permeabilization is a slower process compared to LiDS lysis. In figure 39, the calcein transportation into the side channel occurs synchronously with the release of the calcein in the main channel. This indicates a gradual permeabilization, where the calcein is contained and progressively released. On the contrary, figure 41 shows a more "aggressive" permeabilization, causing the cell to release its content in the main channel before transportation. This is observed from the delayed intensity increase in the analysis channel with respect to the high intensity in the the main channel. Subsequently, when the membrane sealing the analysis channel aperture is lysed, free solution exchange between the main channel and analysis channel can be established which is shown by the depletion of intensity in the main channel.

Using an EOF driven by an electric field of 317 V/cm (as done with LiDS lysis), instead of 32 V/cm (as done with digitonin permeabilization) results in a higher efficiency of cell content transportation. This is shown with a higher flow rate combined with a larger amount of calcein transported. This high flow rate can become a problem if the analys following cell sampling requires hybridyzation of molecules on an array. Therefore, the experiment with the low flow rate provides a good proof-of-principle for a mechanism of cell content transportation with the capacity of being applied in a hybridization based assay for biomolecule analysis. The larger amount of cell content that is transported with the 317 V/cm driven EOF is not very interesting if sensors for single molecule detection are employed. The only advantage of using a high electric field, is the restriction of the diffusion time after lysis.

A completely different situation arises if a cell does not completely seal the aperture due to a particle, as shown in figure 37C. The voltage drop accross the aperture decreases and transportation of sample from the main channel to the analysis channel becomes easier. For the EOF establishment, 200 V is used. This provides an electric field strength of 127 V/cm in the analysis channels. Again, the time measurement starts upon detection of the flow in the analysis channel. Figure 42 shows the calcein transportation in the analysis channel after cell lysis. Since the cell trapping is similar to mode 1, the lysis is expected to be largely homogeneous. This will result in fast transportation of the cell content after the membrane is disrupted. Moreover, the incomplete sealing of the analysis channel aperture allows fast transportation of the released calcein from the main channel into the analysis channel. This time-dependency is shown in figure 43 by measuring the fluorescence intensity in the analysis channel and main channel using ImageJ.

After application of the electric field, the fluorescence intensity in the analysis channel initially decreases while it increases in the main channel, indicating that a small amount of released calcein is transported away from the cell in the analysis channel while the LiDS is still disrupting the membrane in the main channel. This decrease is followed by a high intensity peak, which is synchronous to the fluorescence intensity peak in the main channel. This indicates that the cell is rapidly releasing calcein and that the solution exchange between the main channel and the analysis channel is instantaneous. This also means, that the cell content is continuously mixed with other biomolecules from the main channel.

Figures 39 (digitonin permeabilization), 41 (LiDS lysis, mode 2) and 43 (LiDS lysis, mode 1) show three distinct profiles for the solution exchange. They all exhibit a different probability of transporting the biomolecules of interest from the trapped cell. The highest probability of transporting the intended molecules into the analysis channel is achieved when using digitonin. The gradual permeabilization ensures that the cell will seal the aperture for the longest period of time, and the chance that a captured biomolecule originates from this cell is therefore high.

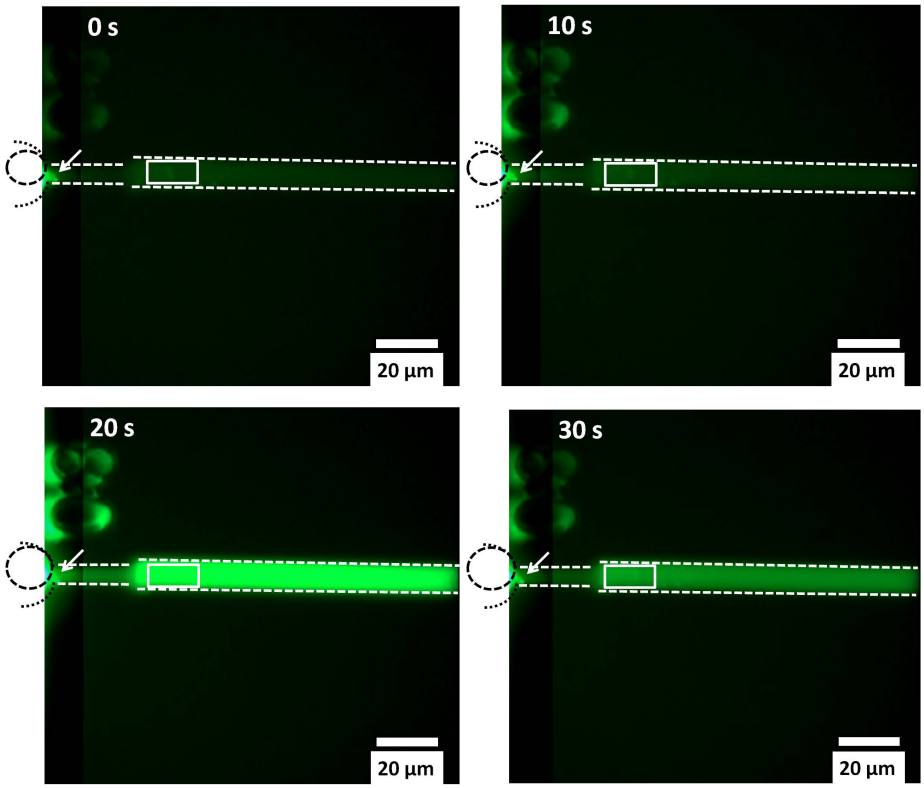

Figure 42: Transportation of calcein from a cell lysed with LiDS. The EOF is established with an electric field strength of 127 V/cm in the side channels and the time interval between two photos is 10 s. In figure 37, it can be seen that the cell does not completely seal the aperture of the trap due to a particle (indicated here with an arrow). The rectangle indicates the area of fluorescence intensity measurement that is used for figure 43.

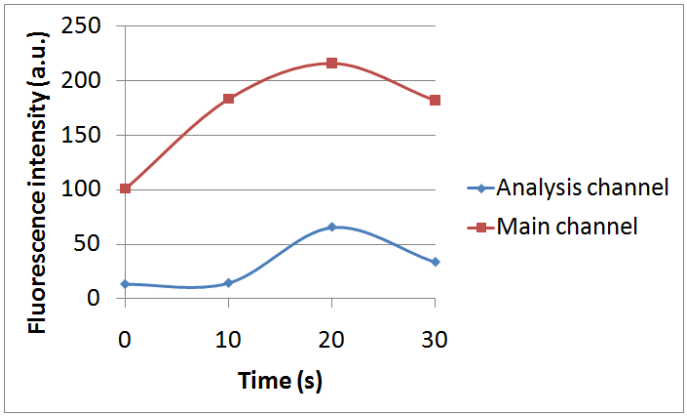

Figure 43: Transportation of calcein after cell lysis with LiDS. The cell does not completely seal the aperture due to a particle, leaving a gap that allows faster transportation of species from the main channel to the analysis channel. Both the fluorescence intensity in the main channel and in the analysis channel are measured using ImageJ (see figure 42) and plotted as a function of the time.

Chemical permeabilization in combination with an EOF results in sampling with loss of biological information due to dilution, but to a much lesser extent than when only chemical permeabilization is employed without an EOF. This EOF is not reproducible, as already mentioned, but

qualitatively this is a proof-of-principle experiment for the application of the EOF for the purpose of cell sampling and it has shown to be a potential useful approach.

A possible implementation exploits both the controlled sample transportation of the EOF and the trapping mode independency of the electrical lysis. This approach offers the advantage that both the lysis and the sampling can be performed with a high control over the lysis-sampling sequence. This also allows automation by programming the appropriate sequence of voltages, e.g., a sequence of 20 s at 1000 V for lysis followed by 1 min at 500 V for analyte transportation.

5 Conclusions and perspectives

The goal of this work on parallel SCA was the development of an integrated microsystem for sampling from individual single cells in parallel. This microchip is intended to be a first prototype and to enable proof-of-principle experiments towards parallel single cell analysis.

Notably, the developed platform is able to perform three of the four main steps of the full protocol for SCA:

- Controllable and reproducible trapping of individual living cells in parallel and at a large scale
- Permeabilization of the plasma membrane in a transient or irreversible manner
- Controlled extraction of the cell content at the single cell level

The last step of the protocol, which has not been investigated here, is the analysis of the extracted biomolecules.

5.1 Chip design and fabrication for parallel trapping of single cells

The microfabricated platform consists of a main channel in which the cells are loaded. Perpendicular to the main channel there is a series of analysis channels, with one channel per cell to be analyzed. The analysis channels are connected to the main channel with dedicated traps. Each trap accomodates one cell and each analysis channel is connected to one trap, allowing parallel single cell analysis.

The cells used in the experiments (P3x65Ag8) are on average 15 μm in diameter, and this average size is taken into account when choosing the dimensions of the structures. The main channel (50 μm high) allows a flow of cells to be easily established. The analysis channels need to be shallow (10 μm) for the optical detection of the released cell content. The traps consist of a pocket in the main channel (20 μm diameter) in which the cell is immobilized, a shallow and narrow constriction (4 μm wide, < 3 μm high) and a connection to the analyis channel. 16 traps are included, which is scalable but this amount allows manual monitoring of cell trapping while showing the capability of parallellization. The length (0 - 30 μm) and the height (2 - 3 μm) of the trap constriction are important parameters for the trapping efficiency.

The analysis channels are connected to one inlet, which is used to apply the negative pressure using dedicated equipment. The optimal pressure is determined to be -30 mbar. The highest trapping efficiency in general (>95%) is achieved when using a short trap constriction (0 μm). Included in this efficiency is single cell trapping as well as the trapping of multiple cells in one trap. This latter phenomenon can occur when the aperture of the constriction is not sealed completely by the first single cell, or when this first cell is too small to fill the trapping pocket properly. These events are not desired. The highest single cell trapping efficiency (90%) is obtained with the short (0 μm) and shallow (2 μm) constriction. In general, the chance of trapping multiple cells is higher when the height of the constriction is increased.

Another interesting phenomenon is the trapping loss, meaning that the cell squeezes through the trap constriction into analysis channels. The highest trapping loss occurs with the same dimensions as determined for the highest single cell trapping efficiency. Whether this loss is a problem or not depends mainly on the amount of cells available for analysis. Either the consequences of the trapping losses need to be handled, or the design has to be adjusted to prevent it. An implementation of the former can be to integrate functionality that removes the cells from the analysis channel prior to the permeabilization. Alternatively, it can be investigated whether decreasing the constriction width (now fixed to 4 μm) reduces the trapping loss. After adjusting for the trapping loss, the highest performance is achieved using shallow traps (60-70%) and this does not depend significantly on the constriction length.

With these results, a fast, controllable and reproducible parallel trapping protocol is established on a platform that is designed for easy scalability. This protocol is amenable to automation,

since cell loading is performed using a passive pumping technique, which will only require a liquid handling robot. Furthermore, the trapping is accomplished using a constant negative pressure from a dedicated controller, a configuration that is not affected by the number of traps. This pressure controller is capable of accurately measuring the flow rate. This can be used as an automated control mechanism for the cell trapping success. For every cell that is trapped, the net flow rate will be reduced with a certain percentage that depends on the number of traps. With the system used, a maximum flow rate of 7 μL/min can be measured with a maximum precision of 1.8 μL/min. In theory, > 3800 levels for the flow rate can be distinghuished, providing the possibility of automatic detection of cell trapping in > 3800 traps.

Another result from this work is the unexpected phenomenon that cells sit in the trap according to two "modes". In mode 1, the cell is sitting in front of the trap constriction, while in mode 2, the cell penetrates the trap constriction. The trapping mode has a significant impact on the results of the subsequent steps of the cell analysis protocol. Unfortunally, the trapping mode is not controllable because it is thought to be related to the cell membrane fluidity. This phenomenon introduces an uncontrollable factor in the cell analysis protocol.

5.2 Cell permeabilization

After the cells have been trapped they are permeabilized using chemicals. Potentially reversible permeabilization using digitonin is successfully demonstrated, but the closing of the pores still need to be shown in future work. The average digitonin permeabilization time is determined to be $\sim$3,5 min. Also, LiDS is used for cell lysis. With this approach, the membrane is destroyed irreversibly in 10 - 20 s.

The permeabilization efficiency depends on the previously mentioned trapping mode. In trapping mode 1, the entire surface of the cell membrane is accesible, leading to homogeneous permeabilization. In trapping mode 2, only the portion of the membrane in the main channel is accessible to the chemicals, leading to partial permeabilization. This result was not expected as an important parameter for cell permeabilization efficiency. Chemical permeabilization is completed in seconds to minutes and this relatively slow process allows biomolecules around the cell to diffuse, leading to a loss of biological information. These results suggest that the chemical permeabilization may not be the best approach.

Alternatively, additional experimentation has been performed using electrical lysis of cells after their trapping. The lysis efficiency turns out to be independent of the trapping mode and the process is completed much faster. This limits the time for diffusion, resulting in less loss of biological information. The hot-spots of the electric field are created in the narrow traps, at the location of the trapped cells. This allows space-specific lysis, avoiding contamination from cells not sitting in the trap but in reservoirs or channels. With the use of an electric field, the cell permeabilization can be done in combination with the EOF transportation of the cell content in the analysis channels. Using LabView, a sequence of voltages can be pre-programmed to automate this combined lysis/sampling process.

In the future, it will be useful to further investigate this electrical approach. This approach would benefit from the past experience of this group (BIOS, University of Twente) with this poration and lysis type [9, 21, 11].

5.3 Cell sampling

With the use of an EOF, the content from the permeabilized individual cells is extracted in the analysis channels, which is demonstrated with calcein transportation. This shows that the ability to recover the cell content after chemical permeabilization is restored when combined with an EOF. When only permeabilization was used, this was not possible. No major influence of the trapping mode is observed.

These results are obtained using proof-of-principle experiments as the established EOF on the chip is not highly controllable. This is due to the varying surface properties of the PDMS. This

must be considered in the future work with the use of other materials or an appropriate surface coating. The EOF needs to be fine-tuned for controlled extraction of cell content and for optimal coupling to the analysis step.

As a conclusion, of this work, a prototype of the microfluidic chip has been developed for parallel SCA with separate protocols for:

1. Reliable, controllable, reproducible, efficient and scalable trapping of living cells
2. Chemical permeabilization of cells (potentially reversible and irreversible)
3. Extraction of the content of the individual cells into analysis channels

Further development will concern the last step of the analysis protocol, with the detection of the target biomolecules.

References

[1] Edgar A. Arriaga. Determining biological noise via single cell analysis. *Analytical and Bioanalytical Chemistry*, 393:73–80, 2009.

[2] Daojing Wang and Steven Bodovitz. Single cell analysis: the new frontier in 'omics'. *Trends in Biotechnology*, 28(6):281–290, 2010.

[3] Andreas Schmid, Hendrik Kortmann, Petra S Dittrich, and Lars M Blank. Chemical and biological single cell analysis. *Current Opinion in Biotechnology*, (21):12–20, 2010.

[4] George M. Whitesides. The origins and the futures of microfluidics. *Nature*, 442:368–373, 2006.

[5] Séverine Le Gac and Albert van den Berg. Single cells as experimentation units in lab-on-a-chip devices. *Trends in Biotechnology*, 28(2):55–62, 2009.

[6] J. Nilsson, M. Evander, B. Hammarström, and T. Laurell. Review of cell and particle trapping in microfluidic systems. *Analytica Chimica Acta*, 649:141–157, 2009.

[7] Robert M. Johann. Cell trapping in microfluidic chips. *Analytical and Bioanalytical Chemistry*, 385:408–412, 2006.

[8] Bruce Alberts, Dennis Bray, Karen Hopkin, Alexander Johnson, Julian Lewis, Martin Raff, Keith Roberts, and Peter Walter. *Essential Cell Biology, second edition*. Garland Science, New York and London, 2004.

[9] Iris van Uitert, Séverine Le Gac, and Albert van den Berg. The influence of different membrane components on the electrical stability of bilayer lipid membranes. *Biochimica et Biopohysica Acta*, 1798:21–31, 2010.

[10] Lucie Kalvodova, Julio L. Sampaio, Sandra Cordo, Christer S. Ejsing, Andrej Shevchenko, and Kai Simons. The lipodomes of vesicular stomatitis virus, semliki forest virus, and the host plasma membrane analyzed by quantitative shotgun mass spectrometry. *Journal of Virology*, 83(16):7996–8003, 2009.

[11] Ana Valero. *Single Cell Electroporation on Chip*. University of Twente, Enschede, The Netherlands, 2006.

[12] Ari Helenius and Kai Simons. Solubilization of membranes by detergents. *Biochimica et Biophysica acta*, 415:29–79, 1975.

[13] Javier Ruiz, Felix M. Goni, and Alicia Alonso. Surfactant-induced release of liposomal contents. a survey of methods and results. *Biochimica et Biophysica Acta*, 937(10):127–134, 1988.

[14] Hasna Ahyayauch, Mohammed Bennouna, Alicia Alonso, and Felix Goni. Detergent effects on membranes at subsolubilizing concentrations: Transmembrane lipid motion, bilayer permeabilization, and vesicle lysis/reassembly are independent phenomena. *Langmuir*, 26(10):7307–7313, 2010.

[15] Kei Miyamoto, Teruyoshi Yamashita, Tomoyuki Tsukiyama, Naoya Kitamura, Naojiro Minami, Masayasu Yamada, and Hiroshi Imai. Reversible membrane permeabilization of mammalian cells treated with digitonin and its use for inducing nuclear reprogramming by xenopus egg extracts. *Cloning and Stem Cells*, 10(4), 2008.

[16] Jessica Olofsson, Helen Bridle, Aldo Jesorka, Ida Isaksson, Stephen Weber, and Owe Orwar. Direct access and control of the intracellular solution environment in single cells. *Analytical Chemistry*, 81(5):1810–1818, 2009.

[17] Math J.H. Geelen. The use of digitonin-permeabilized mammalian cells for measuring enzyme activities in the course of studies on lipid metabolism. *Analytical Biochemistry*, 347:1–9, 2005.

[18] Hua Pan, Yun Zhou, Olivier Izadnegahdar, Jianmin Cui, and Cheri X. Deng. Study of sonoporation dynamics affected by ultrasound duty cycle. *Ultrasound in Medicine and Biology*, 31(6):849–856, 2005.

[19] Herbert Schneckenburger, Anita Hendinger, Reinhard Sailer, Wolfgang S. L. Strauss, and Michael Schmitt. Laser-assisted optoporation of single cells. *J. Biomedical Optics*, 410(7), 2002.

[20] Séverine Le Gac, Ed Zwaan, Albert van den Berg, and Claus-Dieter Ohl. Sonoporation of suspension cells with a single cavitation bubble in a microfluidic confinement. *Lab on a Chip*, 7:1666–1672, 2007.

[21] Iris van Uitert, Séverine Le Gac, and Albert van den Berg. Determination of the electroporation onset of bilayer lipid membranes as a novel approach to establish ternary phase diagrams: example of the l-α-pc/sm/cholesterol system. *Soft Matter*, 6:4420–4429, 2010.

[22] Séverine Le Gac, Drs. N. Bontoux, and M.C. Potier. *Analysis of proteins at the single cell level in "Unraveling single cell genomics"*. RSC Publisher, 2010.

[23] Songyue Chen, Johan G. Bomer, Wilfred G. van der Wiel, Edwin T. Carlen, and Albert van den Berg. Top-down fabrication of sub-30 nm monocrystalline silicon nanowires using conventional microfabrication. *ACS Nano*, 3(11):3485–3492, 2009.

[24] Yu Chang Kim, Seung-Hoon Kim, Duckjong Kim, Sang-Jin Park, and Je-Kyun Park. Plasma extraction in a capillary-driven microfluidic device using surfactant-added poly(dimethylsiloxane). *Sensors and Actuators B*, 145:861–868, 2010.

[25] Glenn M. Walker and David J. Beebe. A passive pumping method for microfluidic devices. *Lab on a Chip*, 2:131–134, 2002.

[26] Tasos C. Papanastasiou, Georgios C. Georgiou, and Andreas N. Alexandrou. *Viscous Fluid Flow*. CRC Press, 1999.

[27] W.E. Morf, O.T. Guenat, and N.F. de Rooij. Partial electroosmotic pumping in complex capillary systems part 1: Principles and general theoretical approach. *Sensors and Actuators B*, 72:266–272, 2001.

[28] Vishal Tandon, Sharath K. Bhagavatula, Wyatt C. Nelson, and Brian J. Kirby. Zeta potential and electroosmotic mobility in microfluidic devices fabricated from hydrophobic polymers: 1. the origins of charge. *Electrophoresis*, 25:1092–1101, 2008.

[29] Alice Sze, David Erickson, Liqing Ren, and Dongqing Li. Zeta-potential measurement using the smoluchoqski equation and the slope of the current-time relationship in electroosmotic flow. *Journal of Colloid and Interface Science*, 261:402–410, 2003.

[30] Tiina Sikanen, Susanne K. Wiedmer, Liisa Heikkilä, Sami Franssila, Risto Kostiainen, and Tapio Kotiaho. Dynamic coating of su-8 microfluidic chips with phospholipid disks. *Electrophoresis*, 31:2566–2574, 2010.

[31] Walter Schrott, Zdenek Slouka, Petr Cervenka, Jiri Ston, Marek Nebyla, Michal Pribyl, and Dalimil Snita. Study on the surface properties of pdms microfluidic chips treated with albumin. *Biomicrofluidics*, 3, 2009.

A Calculation of the hydrodynamic flow resistance

A channel section has a hydrodynamic resistance R_h, which is defined as the ratio of the pressure difference (ΔP) accross the channel and volumetric flow rate (Q) through the channel:

$$R_h = \frac{\Delta P}{Q} \tag{21}$$

In which

$$\Delta P = -\frac{\partial P}{\partial x} l \tag{22}$$

Figure 10 indicates these parameters ($\Delta P = P_{high} - P_{low}$).

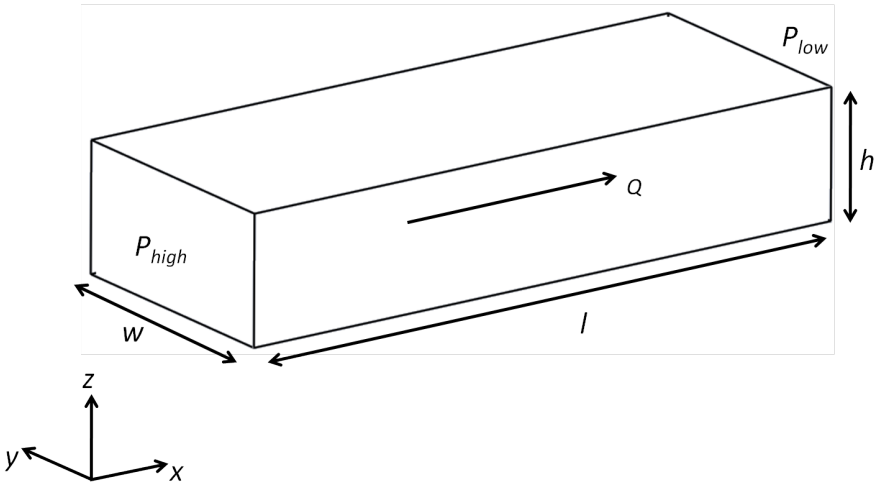

Figure 44: Fluidic channel section (dimensions l, w and h) with a pressure difference $\Delta P = P_{high} - P_{low}$ and a volumetric flow rate Q.

The pressure acts solely in the x-direction, resulting in a flow in the x-direction only which is laminar and fully developed. The flow velocity profile in y and z is described by the Poisson equation:

$$\frac{\partial^2 u_x}{\partial y^2} + \frac{\partial^2 u_x}{\partial z^2} = \frac{1}{\eta}\frac{\partial P}{\partial x} \tag{23}$$

The following boundary conditions are employed:

$$\begin{aligned} \frac{\partial u_x}{\partial y} &= 0 \qquad y = 0 \\ u_x &= 0 \qquad y = w \\ \frac{\partial u_x}{\partial z} &= 0 \qquad z = 0 \\ u_x &= 0 \qquad z = h \end{aligned}$$

These equations are solved for $u_x(y,z)$ in the work of [26] to find the the velocity profile in the y and z direction of the flow in the x direction:

$$u_x(y,z) = -\frac{h^2}{2\eta}\frac{\partial P}{\partial x}\left[1 - \left(\frac{z}{h}\right)^2 + \frac{32}{\pi^3}\sum_{m=0}^{\infty}\frac{(-1)^{m+1}}{(2m+1)^3}\frac{cosh(\frac{(2m+1)\pi y}{2h})}{cosh(\frac{(2m+1)\pi w}{2h})}cos\left(\frac{(2m+1)\pi z}{2h}\right)\right] \tag{24}$$

When the width increases, the profile becomes more horizontal, and the dependency of $u_x(y,z)$ on y decreases.

The volumetric flow velocity Q, which is needed to calculate the channel resistance, follows from integration of the flow velocity over the y-z plane:

$$\int_0^w \int_0^h u_x(y,z)dzdy \tag{25}$$

This is also done in [26], resulting in:

$$Q = -\frac{h^3 w}{12\eta}\frac{\partial P}{\partial x}\left[1 - \frac{192h}{\pi^5 w}\sum_{m=0}^{\infty}\frac{tanh\left(\frac{(2m+1)\pi w}{2h}\right)}{(2m+1)^5}\right] \tag{26}$$

and by combining equation 4 and 26 in 3, the channel resistance is obtained:

$$R_h = \frac{12\eta l}{h^3 w\left[1 - \frac{192h}{\pi^5 w}\sum_{m=0}^{\infty}\frac{tanh\left(\frac{(2m+1)\pi w}{2h}\right)}{(2m+1)^5}\right]} \tag{27}$$

In order to use the channel resistance in practical calculations, the conditional approximation is made for R_h [27]:

$$R_h \approx \frac{12\eta l}{h^3(w - 0.63h)} \qquad w \geq h \tag{28}$$